DES-2023-805
FERMILAB-PUB-23-0821-PPD

Draft version January 2, 2024
Typeset using LaTeX **twocolumn** style in AASTeX631

EMBARGOED UNTIL JAN. 8, 2024 at 2:00 CT

The Dark Energy Survey: Cosmology Results With ∼1500 New High-redshift Type Ia Supernovae Using The Full 5-year Dataset

T. M. C. Abbott,[1] M. Acevedo,[2] M. Aguena,[3] S. Allam,[4] J. Annis,[4] P. Armstrong,[5] J. Asorey,[6] S. Avila,[7] D. Bacon,[8] K. Bechtol,[9] P. H. Bernardinelli,[10] G. M. Bernstein,[11] E. Bertin,[12,13] S. Bocquet,[14] D. Brooks,[15] D. Brout,[6,16] D. L. Burke,[17,18] R. Camilleri,[19] A. Carnero Rosell,[20,3,21] J. Carretero,[7] F. J. Castander,[22,23] R. Cawthon,[24] R. Chen,[25] C. Conselice,[26,27] M. Costanzi,[28,29,30] L. N. da Costa,[3] M. E. S. Pereira,[31] T. M. Davis,[19] S. Desai,[32] M. Dixon,[33] S. Dodelson,[34,35] P. Doel,[15] C. Doux,[11,36] I. Ferrero,[37] B. Flaugher,[4] J. Frieman,[4,38] L. Galbany,[22,23] J. García-Bellido,[39] M. Gatti,[11] G. Giannini,[7,38] K. Glazebrook,[33] O. Graur,[8] D. Gruen,[14] R. A. Gruendl,[40,41] G. Gutierrez,[4] K. Herner,[4] S. R. Hinton,[19] D. L. Hollowood,[42] D. Huterer,[43] D. J. James,[16] R. Kessler,[44,38] K. Kuehn,[45,46] J. Lee,[11] G. F. Lewis,[47] H. Lin,[4] J. L. Marshall,[48] P. Martini,[49,50] J. Mena-Fernández,[51] F. Menanteau,[40,41] R. Miquel,[52,7] J. Mould,[33] E. Neilsen,[4] R. C. Nichol,[8] P. Nugent,[53] R. L. C. Ogando,[54] A. Palmese,[34] M. Paterno,[4] A. Pieres,[3,54] A. A. Plazas Malagón,[17,18] A. Porredon,[55] H. Qu,[11] A. K. Romer,[56] A. Roodman,[17,18] B. Rose,[25] B. O. Sánchez,[57] E. Sanchez,[58] D. Sanchez Cid,[58] D. Scolnic,[25] I. Sevilla-Noarbe,[58] M. Smith,[59] M. Soares-Santos,[6,43] E. Suchyta,[60] M. Sullivan,[59] G. Tarle,[43] C. To,[49] B. E. Tucker,[5] D. L. Tucker,[4] M. Vincenzi,[8,59] A. R. Walker,[1] N. Weaverdyck,[43,53] J. Weller,[61,62] P. Wiseman,[59] F. Yuan,[5] and Y. Zhang[1]

[1] *Cerro Tololo Inter-American Observatory, NSF's National Optical-Infrared Astronomy Research Laboratory, Casilla 603, La Serena, Chile*

[2] *Department of Physics, Duke University, Durham, NC 27708, USA*

[3] *Laboratório Interinstitucional de e-Astronomia - LIneA, Rua Gal. José Cristino 77, Rio de Janeiro, RJ - 20921-400, Brazil*

[4] *Fermi National Accelerator Laboratory, P. O. Box 500, Batavia, IL 60510, USA*

[5] *The Research School of Astronomy and Astrophysics, Australian National University, ACT 2601, Australia*

[6]

[7] *Institut de Física d'Altes Energies (IFAE), The Barcelona Institute of Science and Technology, Campus UAB, 08193 Bellaterra (Barcelona) Spain*

[8] *Institute of Cosmology and Gravitation, University of Portsmouth, Portsmouth, PO1 3FX, UK*

[9] *Physics Department, 2320 Chamberlin Hall, University of Wisconsin-Madison, 1150 University Avenue Madison, WI 53706-1390*

[10] *Astronomy Department, University of Washington, Box 351580, Seattle, WA 98195, USA*

[11] *Department of Physics and Astronomy, University of Pennsylvania, Philadelphia, PA 19104, USA*

[12] *CNRS, UMR 7095, Institut d'Astrophysique de Paris, F-75014, Paris, France*

[13] *Sorbonne Universités, UPMC Univ Paris 06, UMR 7095, Institut d'Astrophysique de Paris, F-75014, Paris, France*

[14] *University Observatory, Faculty of Physics, Ludwig-Maximilians-Universität, Scheinerstr. 1, 81679 Munich, Germany*

[15] *Department of Physics & Astronomy, University College London, Gower Street, London, WC1E 6BT, UK*

[16] *Center for Astrophysics | Harvard & Smithsonian, 60 Garden Street, Cambridge, MA 02138, USA*

[17] *Kavli Institute for Particle Astrophysics & Cosmology, P. O. Box 2450, Stanford University, Stanford, CA 94305, USA*

[18] *SLAC National Accelerator Laboratory, Menlo Park, CA 94025, USA*

[19] *School of Mathematics and Physics, University of Queensland, Brisbane, QLD 4072, Australia*

[20] *Instituto de Astrofisica de Canarias, E-38205 La Laguna, Tenerife, Spain*

[21] *Universidad de La Laguna, Dpto. Astrofísica, E-38206 La Laguna, Tenerife, Spain*

[22] *Institut d'Estudis Espacials de Catalunya (IEEC), 08034 Barcelona, Spain*

[23] *Institute of Space Sciences (ICE, CSIC), Campus UAB, Carrer de Can Magrans, s/n, 08193 Barcelona, Spain*

[24] *Physics Department, William Jewell College, Liberty, MO, 64068*

[25] *Department of Physics, Duke University Durham, NC 27708, USA*

[26] *Jodrell Bank Center for Astrophysics, School of Physics and Astronomy, University of Manchester, Oxford Road, Manchester, M13 9PL, UK*

[27] *University of Nottingham, School of Physics and Astronomy, Nottingham NG7 2RD, UK*

[28] *Astronomy Unit, Department of Physics, University of Trieste, via Tiepolo 11, I-34131 Trieste, Italy*

[29] *INAF-Osservatorio Astronomico di Trieste, via G. B. Tiepolo 11, I-34143 Trieste, Italy*

[30] *Institute for Fundamental Physics of the Universe, Via Beirut 2, 34014 Trieste, Italy*

[31] *Hamburger Sternwarte, Universität Hamburg, Gojenbergsweg 112, 21029 Hamburg, Germany*

[32] *Department of Physics, IIT Hyderabad, Kandi, Telangana 502285, India*

[33] *Centre for Astrophysics & Supercomputing, Swinburne University of Technology, Victoria 3122, Australia*

[34] *Department of Physics, Carnegie Mellon University, Pittsburgh, Pennsylvania 15312, USA*

[35] *NSF AI Planning Institute for Physics of the Future, Carnegie Mellon University, Pittsburgh, PA 15213, USA*
[36] *Université Grenoble Alpes, CNRS, LPSC-IN2P3, 38000 Grenoble, France*
[37] *Institute of Theoretical Astrophysics, University of Oslo. P.O. Box 1029 Blindern, NO-0315 Oslo, Norway*
[38] *Kavli Institute for Cosmological Physics, University of Chicago, Chicago, IL 60637, USA*
[39] *Instituto de Fisica Teorica UAM/CSIC, Universidad Autonoma de Madrid, 28049 Madrid, Spain*
[40] *Center for Astrophysical Surveys, National Center for Supercomputing Applications, 1205 West Clark St., Urbana, IL 61801, USA*
[41] *Department of Astronomy, University of Illinois at Urbana-Champaign, 1002 W. Green Street, Urbana, IL 61801, USA*
[42] *Santa Cruz Institute for Particle Physics, Santa Cruz, CA 95064, USA*
[43] *Department of Physics, University of Michigan, Ann Arbor, MI 48109, USA*
[44] *Department of Astronomy and Astrophysics, University of Chicago, Chicago, IL 60637, USA*
[45] *Australian Astronomical Optics, Macquarie University, North Ryde, NSW 2113, Australia*
[46] *Lowell Observatory, 1400 Mars Hill Rd, Flagstaff, AZ 86001, USA*
[47] *Sydney Institute for Astronomy, School of Physics, A28, The University of Sydney, NSW 2006, Australia*
[48] *George P. and Cynthia Woods Mitchell Institute for Fundamental Physics and Astronomy, and Department of Physics and Astronomy, Texas A&M University, College Station, TX 77843, USA*
[49] *Center for Cosmology and Astro-Particle Physics, The Ohio State University, Columbus, OH 43210, USA*
[50] *Department of Astronomy, The Ohio State University, Columbus, OH 43210, USA*
[51] *LPSC Grenoble - 53, Avenue des Martyrs 38026 Grenoble, France*
[52] *Institució Catalana de Recerca i Estudis Avançats, E-08010 Barcelona, Spain*
[53] *Lawrence Berkeley National Laboratory, 1 Cyclotron Road, Berkeley, CA 94720, USA*
[54] *Observatório Nacional, Rua Gal. José Cristino 77, Rio de Janeiro, RJ - 20921-400, Brazil*
[55] *Ruhr University Bochum, Faculty of Physics and Astronomy, Astronomical Institute, German Centre for Cosmological Lensing, 44780 Bochum, Germany*
[56] *Department of Physics and Astronomy, Pevensey Building, University of Sussex, Brighton, BN1 9QH, UK*
[57] *Centre de Physique des Particules de Marseille, 163 Av. de Luminy, CEDEX 09, Marseille, France*
[58] *Centro de Investigaciones Energéticas, Medioambientales y Tecnológicas (CIEMAT), Madrid, Spain*
[59] *School of Physics and Astronomy, University of Southampton, Southampton, SO17 1BJ, UK*
[60] *Computer Science and Mathematics Division, Oak Ridge National Laboratory, Oak Ridge, TN 37831*
[61] *Max Planck Institute for Extraterrestrial Physics, Giessenbachstrasse, 85748 Garching, Germany*
[62] *Universitäts-Sternwarte, Fakultät für Physik, Ludwig-Maximilians Universität München, Scheinerstr. 1, 81679 München, Germany*

ABSTRACT

We present cosmological constraints from the sample of Type Ia supernovae (SN Ia) discovered and measured during the full five years of the Dark Energy Survey (DES) Supernova Program. In contrast to most previous cosmological samples, in which supernovae are classified based on their spectra, we classify the DES supernovae using a machine learning algorithm applied to their light-curves in four photometric bands. Spectroscopic redshifts are acquired from a dedicated follow-up survey of the host galaxies of the SNe. After accounting for the likelihood of a SN being a SN Ia, we find 1635 DES supernovae in the redshifts $0.10 < z < 1.13$ that pass quality selection criteria and can be used to constrain cosmological parameters. This quintuples the number of high-quality $z > 0.5$ supernovae compared to the previous leading compilation of Pantheon+, and results in the tightest cosmological constraints achieved by any supernova data set to date. To derive cosmological constraints we combine the DES supernova data with a high-quality external low-redshift sample consisting of 194 SNe Ia spanning $0.025 < z < 0.10$. Using supernova data alone and including systematic uncertainties we find $\Omega_{\rm m} = 0.352 \pm 0.017$ in a flat ΛCDM model, and $(\Omega_{\rm m}, w) = (0.264^{+0.074}_{-0.096}, -0.80^{+0.14}_{-0.16})$ in a flat wCDM model. For a $w_0 w_a$CDM model, we find $(\Omega_{\rm m}, w_0, w_a) = (0.495^{+0.033}_{-0.043}, -0.36^{+0.36}_{-0.30}, -8.8^{+3.7}_{-4.5})$, consistent with a constant equation of state parameter to within $\sim 2\sigma$. Including Planck Cosmic Microwave Background data, SDSS Baryon Acoustic Oscillation data, and DES 3×2-point data gives $(\Omega_{\rm m}, w) = (0.321 \pm 0.007, -0.941 \pm 0.026)$. In all cases dark energy is consistent with a cosmological constant to within approximately 2σ. In our analysis, systematic errors on cosmological parameters are subdominant compared to statistical errors; these results thus pave the way for future photometrically classified supernova analyses such as those planned for the Vera C. Rubin Observatory's Legacy Survey of Space and Time.

Keywords: supernovae, cosmology, dark energy

1. INTRODUCTION

The standard cosmological model posits that the energy density of the Universe is dominated by dark components that have not been detected in terrestrial experiments and thus do not appear in the standard model of particle physics. Known as cold dark matter and dark energy, their study represents an opportunity to deepen our understanding of fundamental physics.

The Dark Energy Survey (DES) was conceived to characterize the properties of dark matter and dark energy with unprecedented precision and accuracy through four primary observational probes (The Dark Energy Survey Collaboration 2005; Bernstein et al. 2012; Dark Energy Survey Collaboration 2016; Lahav et al. 2020). One of these four probes is the Hubble diagram (redshift-distance relation) for Type Ia supernovae (SNe Ia), which constrains the history of the cosmic expansion rate. To implement this probe, the DES SN survey was designed to provide the largest, most homogeneous sample of high-redshift supernovae ever discovered. The two papers that first presented evidence for the accelerated expansion of the universe (Riess et al. 1998; Perlmutter et al. 1999) used a total of 52 high-redshift supernovae with sparsely sampled light-curve measurements in one or two optical passbands. We present here the cosmological constraints using the full 5-year DES SN dataset, consisting of well-sampled, precisely calibrated light curves for 1635 new high-redshift supernovae observed in four bands g, r, i, z.

For the last decade, SN Ia cosmology constraints have largely come from combining data from many surveys. The recent Pantheon+ analysis (Scolnic et al. 2022; Brout et al. 2022a) combined three separate mid-z samples ($0.1 < z < 1.0$), 11 different low-z samples ($z < 0.1$), and four separate high-z samples ($z > 1.0$), each with different photometric systems and selection functions (Gilliland et al. 1999; Hicken et al. 2009; Riess et al. 2001, 2004, 2007; Sullivan et al. 2011; Hicken et al. 2012; Suzuki et al. 2012; Ganeshalingam et al. 2013; Betoule et al. 2014; Krisciunas et al. 2017; Foley et al. 2017; Riess et al. 2018; Sako et al. 2018; Brout et al. 2019b; Smith et al. 2020a). The DES sample, which rivals in number the entirety of Pantheon+, does not have the low-redshift ($z < 0.1$) coverage to completely remove the need for external low-z samples, but at higher redshift enables us to replace a heterogeneous mix of samples with a homogeneous sample of high quality, well-calibrated light-curves.

One of the aims of the DES analysis was to minimize systematic (relative to statistical) errors to enable a robust analysis. Vincenzi & The Dark Energy Survey (2024) shows that our error budget is dominated by statistical uncertainty, in contrast to most SN cosmology analyses of the last decade, for which the systematic uncertainties equalled or exceeded the statistical uncertainties (Betoule et al. 2014; Scolnic et al. 2018; Dark Energy Survey Collaboration 2019). We also highlight that the most critical sources of systematics are those related to the lack of a homogeneous and well calibrated low-z sample.

As the DES sample enables a SN Ia measurement of cosmological parameters that is largely independent of previous SN cosmology analyses, we have been careful to 'blind' our analysis. The analysis work described in Vincenzi & The Dark Energy Survey (2024), which stops just short of constraining cosmological parameters, was shared widely with the DES collaboration, evaluated, and approved before unblinding. Unblinding standards included multiple validation checks with simulations and full accounting and explanation of the error budget. No elements of the analysis were changed after unblinding.

In this paper we review the analysis of the complete DES SN dataset (as detailed in many supporting papers; see Fig. 1) and present the cosmological results. An important advance on most previous analyses is that we use a photometrically classified rather than spectroscopically classified sample, and implement advanced techniques to classify SN Ia and incorporate classification probabilities in the cosmological parameter estimation (Möller & de Boissière 2020; Qu et al. 2021; Kunz et al. 2012; Hlozek et al. 2012). While this increases the complexity of the analysis, in this work and previous papers (Vincenzi et al. 2023; Möller et al. 2022) we show that the impact of contamination due to photometric misclassification is well below the statistical uncertainty on cosmological parameters, and this constitutes one of the key results of our analysis. Combining our DES data with a low-redshift sample (see Sect. 2), we fit the Hubble diagram to test the standard cosmological model as well as multiple common extensions including spatial curvature, non-vacuum dark energy, and dark energy with an evolving equation of state parameter. In Camilleri et al. (in prep. 2024) we present fits to more exotic models.

The structure of the paper is as follows. We begin in Sec. 2 by describing the dataset, its acquisition, reduction, calibration, and light-curve fitting. We summarise the models we test in Sec. 3 before presenting the results

DES-SN5YR analysis overview

Data:
- Calibration (Burke et al. 2018, Brout et al. 2022, Rykoff et al. 2023)
- SN photometry (Brout et al. 2019, Sanchez et al. 2024)
- SN spectroscopy (Smith et al. 2020a)
- DCR and chrom (Lasker et al. 2018, Lee&Acevedo et al. 2023)
- Host galaxy redshifts and properties (Lidman et al. 2020, Carr et al. 2021, Wiseman et al. 2020/2021, Kelsey et al. 2023)

Simulations:
- Survey selection effects (Kessler et al. 2019, Vincenzi et al. 2020)
- SN Ia intrinsic and dust properties (Brout&Scolnic 2021, Popovic et al. 2021a/b, Wiseman et al. 2022) and rates (Wiseman et al. 2021)
- Contamination (Vincenzi et al. 2020)

Analysis:
Pipeline and Overview (Hinton et al. 2020, Vincenzi et al. 2024)
- Light-curve fitting (Taylor et al. 2023)
- SN classification (Möller & de Boissière 2020, Qu et al. 2021, Vincenzi et al. 2021, Moller et al. 2022)
- "BEAMS" and bias corrections (Kessler et al. 2017) and unbinning the SN covariance matrix (Brout et al. 2020, Kessler et al. 2023)
- Effects of host galaxy mismatch (Qu et al. 2023)
- Cosmological contour validation (Armstrong et al. 2023)

Cosmological results: DES Collaboration 2024
Testing non-standard cosmological models (Camilleri et al. 2024)

Figure 1. Overview of the papers that fed into these cosmological results.

in Sec. 4; our discussion and conclusions follow in Sec. 5 and Sec. 6. The details of our data release, which includes the code needed to reproduce our results, appear in Sánchez (in prep. 2024).

2. DATA AND ANALYSIS

2.1. *DES and Low-redshift SNe*

Our primary dataset is the full five years of DES SNe, which we combine with a historical set of nearby supernovae from CfA3 (Hicken et al. 2009), CfA4 (Hicken et al. 2012), CSP (Krisciunas et al. 2017, DR3) and the Foundation SN sample (Foley et al. 2017). We refer to the combined DES plus historical dataset as **DES-SN5YR**.

The DES supernova program was carried out over five seasons, August to February from 2013–2018, during which we observed ten $\sim 3\,\mathrm{deg}^2$ fields with approximately weekly cadence in four bands (g, r, i, z). Eight of the fields were observed to an r-magnitude of $m_r \leq 23.5$ (shallow fields) and two to a deeper limit of $m_r \leq 24.5$ (deep fields). See Smith et al. (2020a) for a summary of the supernova program and Diehl et al. (2016); **?** for observational details.

The DES SNe were discovered via difference imaging (Kessler et al. 2015) based on the method of Alard & Lupton (1998). DES images are calibrated following the Forward Global Calibration Method (FGCM; Burke et al. 2018; Sevilla-Noarbe et al. 2021; Rykoff 2023), and both DES and low-z samples are recalibrated as part of the SuperCal-Fragilistic cross calibration effort described in Brout et al. (2022b). SN fluxes are determined using scene modeling photometry (Brout et al. 2019b); we include corrections from spectral energy distribution variations (Lasker et al. 2019) and from differential chromatic refraction and wavelength-dependent seeing (Lee & Acevedo et al. 2023). We estimate the overall accuracy of our calibrated photometry to be $\lesssim 5$ mmag. Host galaxies are assigned following the directional light radius (DLR) method (Sullivan et al. 2006; Gupta et al. 2016; Qu et al. 2023), and host galaxy properties are determined as described by Kelsey et al. (2023) based on Fioc & Rocca-Volmerange (1999) using deep coadded images by Wiseman et al. (2020). Host galaxy spectroscopic redshifts are obtained primarily within the OzDES programme (Yuan et al. 2015; Childress et al. 2017; Lidman et al. 2020). The final data release of photometry of $\sim 20,000$ candidates, redshifts of hosts, and host galaxy properties is presented in Sánchez (in prep. 2024).

We apply strict quality cuts to this sample of candidates to select our final high-quality sample for the Hubble diagram. The same quality cuts were applied to both the low-z sample and the DES supernovae. As a first cut we require a spectroscopic redshift of the host galaxy, good light-curve coverage (at least two detections with SNR> 5 in two different bands), and a well converged light curve fit using the SALT3 model (Kenworthy et al. 2021; Taylor et al. 2023); this reduces the DES sample size to 3621. Additional requirements include light curve parameters (stretch and colour) within normal range for SNe Ia, a well constrained time of peak brightness, good fit-probability, and valid distance-bias correction from our simulation (see Table 4 of Vincenzi & The Dark Energy Survey 2024, for more detail). Our final Hubble-diagram sample includes **1635** supernovae, of which 1499 have a machine-learning probability of being a Type Ia greater than 50% (see Sec. 2.2). Note that we do not perform a cut on this machine-learning probability, rather we use it in the BEAMS procedure that produces our Hubble diagram and to weight the SN distance uncertainties in the fits to the final Hubble diagram (Kessler et al. 2023). The set of all DES light-curves is visualised in Figure 2.

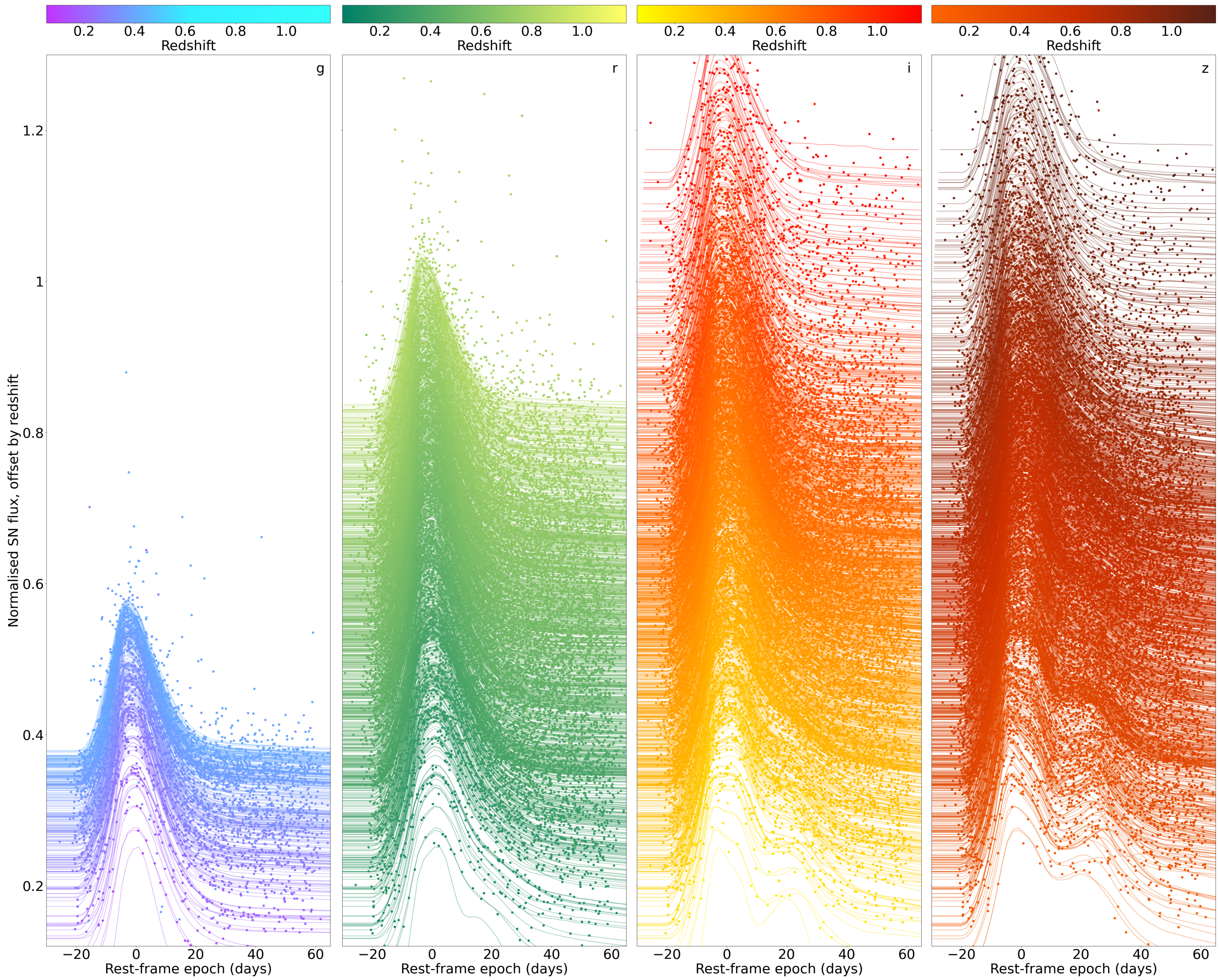

Figure 2. All DES light curves, showing observed magnitudes in g, r, i, and z bands (left to right respectively) normalised by the maximum brightness of each light curve, and with the time-axis de-redshifted to the rest-frame. Each light curve has been arbitrarily offset by their redshift, with higher-redshift objects higher on the plot (as labeled on vertical axis). Lines show best-fit SALT3 light curve fits. The g-band and r-band light curves are not used above $z \sim 0.4$ and $z \sim 0.85$ respectively because that corresponds to the redshifts at which the lower-wavelength limit of the SALT3 model (3500Å in the rest frame) passes out of their observed wavelength ranges.

Since we focus on minimizing potential systematic errors, we only use the best-calibrated, most homogeneous sample of low-z SNe Ia. To reduce the impact of peculiar velocity uncertainties we cut out all SNe with $z < 0.025$. We furthermore combine only a subset of the available low-redshift samples: CfA3&4, CSP, and Foundation SNe, which are the four largest low-z samples with well-understood photometric calibration. Our low-z sample thus totals 194 supernovae with $z < 0.1$; this can be compared to Pantheon+, for which the low-z sample was almost four times larger (741 supernovae at $z < 0.1$). We have thus exchanged the statistical constraining power of more low-z supernovae for better control of systematics. The redshift distribution of our sample compared to the compilation of historical samples in Pantheon+ is shown in Fig. 3. To conclude, the final DES-SN5YR sample includes 1635 DES SNe and 194 low-z external SNe, for a total of **1829** SNe.

2.2. *From light-curves to Hubble diagram*

A critical step in the cosmology analysis is to convert each supernova's light curve (magnitude vs time in multiple bands; see examples in Fig. 2) to a single calibrated number representing its standardised magnitude and estimated distance modulus.

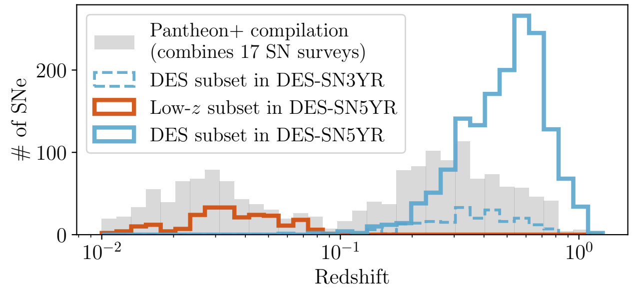

Figure 3. Histogram showing the redshift distribution of the DES-SN5YR sample, with new DES SNe in blue and our low-z sample in red. For comparison the distribution of redshifts in the existing Pantheon+ sample is shown in grey (Brout et al. 2022a), which also includes the DES SNe from the DES-SN3YR analysis (blue dashed line). The five-year DES sample contains $\sim 4\times$ more supernovae above $z \sim 0.4$ than the Pantheon+ compilation.

To achieve this, we use the SALT3 light curve fitting model as presented in Kenworthy et al. (2021); Taylor et al. (2023) and retrained in Vincenzi & The Dark Energy Survey (2024) to determine the light-curve fit parameters, amplitude of the SN flux (x_0), stretch (x_1), and color (c). These fitted parameters are used to estimate the distance modulus, $\mu \equiv m - M$, using an adaptation of the Tripp equation (Tripp 1998) that includes a correction for observed correlations between SN Ia luminosity and host properties, $G_{\rm host}$. This has historically been described as a 'mass step' but we also consider the possibility that it is a 'color step' (see Sec. 2.2 of Vincenzi & The Dark Energy Survey 2024), †

$$\mu_{{\rm obs},i} = m_{x,i} + \alpha x_{1,i} - \beta c_i + \gamma G_{{\rm host},i} - M - \mu_{{\rm bias},i}, \quad (1)$$

where $m_x = -2.5\log_{10}(x_0)$.[1] The constants α, β, and γ are global parameters determined from the likelihood analysis of all the SNe on the Hubble diagram, while the terms subscripted by i refer to parameters of individual SNe. We find $\alpha = 0.161 \pm 0.001$, $\beta = 3.12 \pm 0.03$, and $\gamma = 0.038 \pm 0.007$. We marginalise over the absolute magnitude M (see Sect. 3). The final term in Eq. 1 accounts for selection effects and Malmquist bias.

The nuisance parameters and $\mu_{{\rm bias},i}$ term in Eq. 1 are determined using the BBC framework (Kessler & Scolnic 2017, 'BEAMS with Bias Corrections'). In particular, bias corrections $\mu_{{\rm bias},i}$ are estimated from a large simulation of our sample. The simulation models the rest-frame SN Ia spectral energy distribution (SED) at all phases, SN correlations with host-galaxy properties, SED reddening through an expanding universe, broadband *griz* fluxes, and instrumental noise (see Fig. 1 in Kessler et al. 2019a). Using Eq. 1 there remains intrinsic scatter of ~ 0.1 mag in Hubble residuals. Following the numerous recent studies on understanding and modelling SN Ia dust extinction and progenitors (Wiseman et al. 2021, 2022; Duarte et al. 2022; Dixon et al. 2022; Chen et al. 2022; Meldorf et al. 2023), we model this residual scatter using the dust-based model from Brout & Scolnic (2021); Popovic et al. (2023a), which improves on the previous commonly used models (Guy et al. 2010; Chotard et al. 2011). This intrinsic scatter remains the largest source of systematic uncertainty from the simulation and it requires excellent control of sample selection effects (which are well modelled for DES but poorly understood for the low-z sample).

As we do not spectroscopically classify the SNe and thus expect contamination from core-collapse (CC) supernovae, we perform machine learning light-curve classification on the sample following Vincenzi et al. (2023); Möller et al. (2022). We implement two advanced machine learning classifiers, SuperNNova (Möller & de Boissière 2020) and SCONE (Qu et al. 2021) and use state-of-the-art simulations to model contamination (estimated to be $\sim$ 6.5%, see Table 10 and Sect. 7.1.5 of Vincenzi & The Dark Energy Survey 2024). Classifiers are trained using core-collapse and peculiar SN Ia simulations based on Vincenzi et al. (2021) and using state-of-the-art SED templates by Vincenzi et al. (2019); Kessler et al. (2019b). These DES simulations are the first to robustly reproduce the contamination observed in the data (Vincenzi et al. 2021; Vincenzi & The Dark Energy Survey 2024, Table 10).

For each SN, the trained classifiers assign a probability of being a Type Ia, and these probabilities are included within the BEAMS framework to marginalize over core-collapse contamination and produce the final Hubble Diagram (Kunz et al. 2012; Hlozek et al. 2012). The final DES-SN5YR Hubble diagram is shown in Fig. 4 and includes 1829 SNe.

As discussed in Kessler et al. (2023); Vincenzi & The Dark Energy Survey (2024), the probability that each supernova is a Type Ia ($P_{\rm Ia}$) is incorporated in the BEAMS fit, so is taken into account in the bias correction,[2] and used to calculate a BEAMS probability, $P_{\rm B(Ia)}$ (see Eq. 9 in Kessler et al. 2023). BEAMS probabili-

[1] Traditionally, the apparent B-band magnitude at peak, $m_{\rm B}$, was used instead of the term m_x. However, in the SALT2 and SALT3 models the light curve amplitude is parameterised by the amplitude term $x_0 = 10^{-m'_B/2.5}$ plus an offset that makes m'_B close to the magnitude in the B-band. This updated formalism was introduced by Marriner et al. (2011).

[2] Note that this means that one should *not* apply a cut on $P_{\rm Ia}$ when fitting to our published Hubble diagram, because the bias correction calculation includes that potential contamination.

ties are used to inflate distance uncertainties of likely contaminants by a factor $\propto 1/\sqrt{P_{\mathrm{B(Ia)}}}$ (see Eq. 10 in Vincenzi & The Dark Energy Survey 2024). Therefore, the **released Hubble diagram data includes the inflated distance uncertainties** (see App. A), allowing users to fit the Hubble diagram directly without applying any additional weighting for the probability that each supernova is a Type Ia. We find 75 SNe with $\sigma_{\mu,i,\mathrm{final}} > 1$ mag once this weighting has been applied, and 1331 SNe with $\sigma_{\mu,i,\mathrm{final}} < 0.2$ mag.[3]

Vincenzi & The Dark Energy Survey (2024) stops short of performing cosmological constraints but provides the corrected distance moduli μ along with their uncertainties σ_μ, redshifts for each SN, and a statistical+systematic covariance matrix C, which we describe further in Sec. 3.

Armstrong et al. (2023) presents validation of the cosmological contours produced by our pipeline. Validation that our analysis pipeline is insensitive to the cosmological model assumed in our bias correction simulation appears in Camilleri et al. (in prep. 2024), who also test more exotic cosmological models.

2.3. *Unblinding criteria*

Throughout our analysis, cosmological parameters estimated from *real data* were blinded. We validate our entire pipeline on detailed catalogue-level simulations and unblind the cosmological parameters estimated from *simulations* to test that the input cosmology is recovered. In addition to the many tests described in Vincenzi & The Dark Energy Survey (2024), the final unblinding criteria that our data passed were:

- **Accuracy of simulations:** Reduced χ^2 between the distribution of data and simulations across a variety of observables (redshift, SALT3 parameters and goodness of the fit, maximum signal-to-noise ratio at peak, host stellar mass) is required to be between 0.7 and 3.0 (see Vincenzi & The Dark Energy Survey 2024, Fig. 3-4).
- **Pipeline validation using DES simulations:** Demonstrate that our pipeline recovers the input cosmology. We produce 25 data-size simulated samples (statistically independent) assuming a Flat-ΛCDM universe with best-fit Planck value of Ω_M and analyze them the same way as real data. We fit each Hubble diagram assuming a Flat-wCDM model with a Planck prior and find $w - w_{\mathrm{true}} \simeq 0.001 \pm 0.020$, where w is the mean value of the marginalized posterior of the dark energy equation of state parameter over the 25 samples, and $w_{\mathrm{true}} = -1$ is the model value of that parameter input to the simulation.
- **Validation of contours:** ensuring our uncertainty limits accurately represent the likelihood of the models (Armstrong et al. 2023).
- **Independence of reference cosmology:** ensuring our results are sufficiently independent of cosmological assumptions that enter our bias correction simulations (Camilleri et al. in prep. 2024).

2.4. *Combining SN with other cosmological probes*

We combine the DES-SN5YR cosmological constraints with measurements from other complementary cosmological probes. In particular, we use:

- Cosmic Microwave Background (CMB) measurements of the temperature and polarisation power spectra (TTTEEE) presented by the Planck Collaboration (2020). We use the Python implementation of Planck's 2015 `Plik_lite` (Prince & Dunkley 2019).
- Weak lensing and galaxy clustering measurements from the DES3×2pt year-3 magnitude-limited (MagLim) lens sample (referred to as DES Y3 3×2pt); 3×2-point refers to the simultaneous fit of three 2-point correlation functions, namely galaxy-galaxy, galaxy-lensing, and lensing-lensing correlations (Dark Energy Survey Collaboration 2022, 2023).
- Baryon acoustic oscillation (BAO) measurements as presented in the extended Baryon Oscillation Spectroscopic Survey paper (eBOSS; Dawson et al. 2016; Alam et al. 2021), which adds the BAO results from SDSS-IV (Blanton et al. 2017) to earlier SDSS BAO data. Specifically, we use 'BAO' to refer to the BAO-only measurements from MGS (Ross et al. 2015), BOSS (SDSS-III Alam et al. 2017), eBOSS LRG (Bautista et al. 2021), eBOSS ELG (de Mattia et al. 2021), eBOSS QSO (Hou et al. 2021), and eBOSS Lya (du Mas des Bourboux et al. 2020).

When combining these data we do simultaneous MCMC fits of the relevant data vectors. We present

[3] Applying a binary classification-based cut (SN Ia or not) is not optimal, as it assumes the classification is perfect. However, we test the binary-cut-based approach by using only the 1499 SNe classified with $P_{\mathrm{Ia}} > 0.5$ and assuming they are a pure SN Ia sample, and we show that the measured shift in w is not significant compared to the statistical uncertainties (Table 11 of Vincenzi & The Dark Energy Survey 2024).

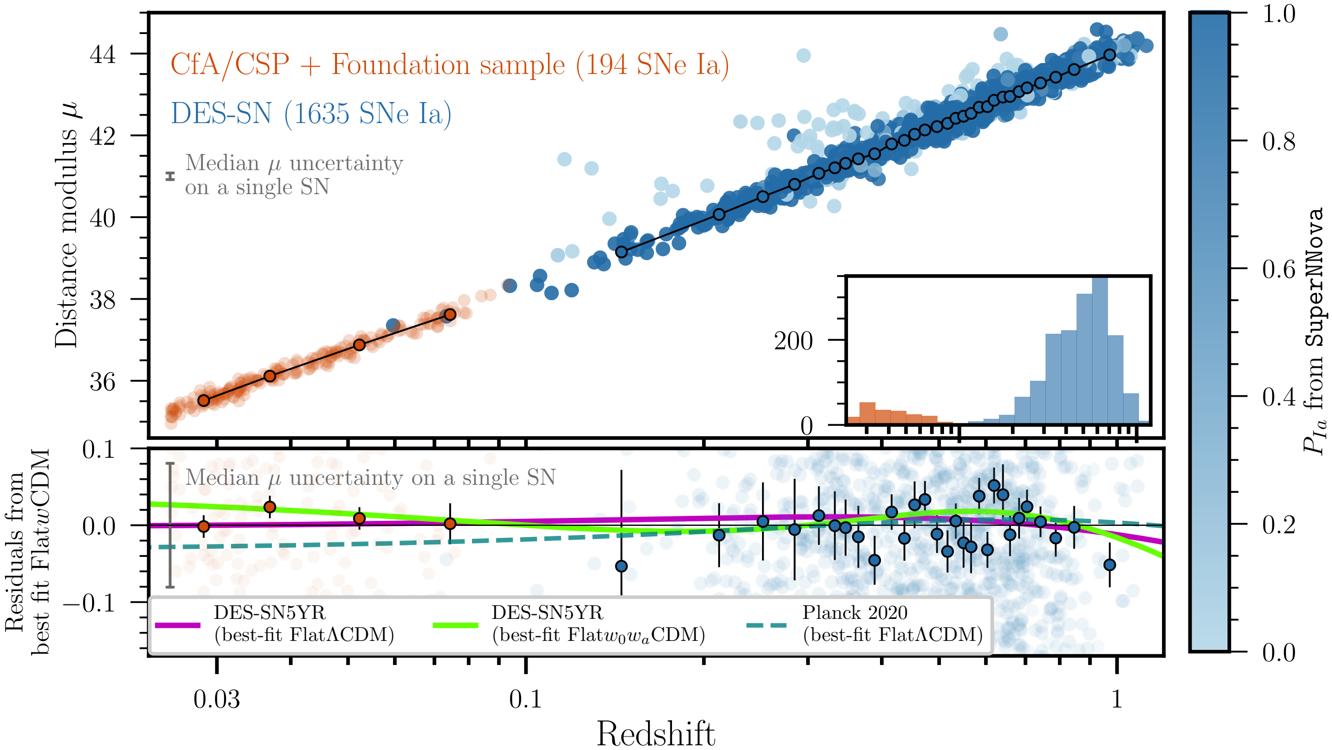

Figure 4. Hubble diagram of DES-SN5YR. We show both the single SN events and the redshift-binned SN distance moduli. Redshift bins are adjusted so that each bin has the same number of SNe (~ 50). The 1635 new DES supernovae are in blue, and in the upper panel they are shaded by their probability of being a Type Ia. It is clear that most outliers are likely contaminants (pale blue). The inset shows the number of SNe in the sample as a function of redshift (same z-range as the main plot). The lower panel subtracts the best fit Flat-wCDM model from DES-SN5YR alone (third result in Table 2), and overplots three other cosmological models — the best fit Flat-ΛCDM model from DES-SN5YR alone (magenta line, first result in Table 2), the best fit Flat-w_0w_aCDM model from DES-SN5YR alone (green line, fourth result in Table 2), and the best fit Planck 2020 Flat-ΛCDM model (dashed line, $\Omega_{\rm m}^{\rm Planck}=0.317\pm0.008$).

three combinations: the simplest CMB-dependent combination CMB+SN, a CMB-independent combination BAO+3×2pt+SN, and a combination of them all.

3. MODELS AND THEORY

We present cosmological results for the standard cosmological model – flat space with cold dark matter and a cosmological constant (Flat-ΛCDM) – and some basic extensions, such as relaxing the assumption of spatial flatness (ΛCDM), allowing for constant equation of state parameter (w) of dark energy (Flat-wCDM), and including a linear parameterisation for time-varying dark energy (Flat-w_0w_aCDM) in which the equation of state parameter is given by $w = w_0 + w_a(1-a)$ (Chevallier & Polarski 2001; Linder 2003).

To calculate the theoretical distance as a function of redshift we begin with the comoving distance,

$$R_0\chi(\bar{z}) = \frac{c}{H_0}\int_0^{\bar{z}} \frac{dz}{E(z)}, \tag{2}$$

where $\bar{z}$ is the redshift due to the expansion of the Universe, $E(z) \equiv H(z)/H_0$ is the normalized redshift-dependent expansion rate and is given for each cosmological model by the expression in Table 1, $R_0 = c/(H_0\sqrt{|\Omega_{\rm k}|})$ is the present day scale factor with dimensions of distance, and the curvature term $\Omega_{\rm k} \equiv 1-\Omega_{\rm m}-\Omega_\Lambda$. The scale factor normalised to the present day is defined as $a \equiv R/R_0$, and the scale factor at the time of emission for an object with cosmological redshift $\bar{z}$ is $a = 1/(1+\bar{z})$. The luminosity distance is given by

$$D_{\rm L}(z_{\rm obs}, \bar{z}) = (1+z_{\rm obs})R_0 S_k(\chi(\bar{z})), \tag{3}$$

where $z_{\rm obs}$ is the observed redshift, and the curvature is captured by $S_k(\chi) = \sin\chi$, χ, and $\sinh\chi$ for closed ($\Omega_k < 0$), flat ($\Omega_k = 0$), and open ($\Omega_k > 0$) universes respectively.[4]

[4] When $\Omega_{\rm k} = 0$ the term $R_0S_k(\chi)$ becomes $R_0\chi$ and can be calculated directly from Eq. 2, bypassing the infinite R_0.

Cosmological Model	Friedmann Equation: $\mathbf{E(z) = H(z)/H_0} =$	Fit Parameters Θ
Flat-ΛCDM	$\left[\Omega_{\rm m}(1+z)^3 + (1-\Omega_{\rm m})\right]^{1/2}$	$\Omega_{\rm m}$
ΛCDM	$\left[\Omega_{\rm m}(1+z)^3 + \Omega_\Lambda + (1-\Omega_{\rm m}-\Omega_\Lambda)(1+z)^2\right]^{1/2}$	$\Omega_{\rm m}, \Omega_\Lambda$
Flat-wCDM	$\left[\Omega_{\rm m}(1+z)^3 + (1-\Omega_{\rm m})(1+z)^{3(1+w)}\right]^{1/2}$	$\Omega_{\rm m}, w$
Flat-w_0w_aCDM	$\left[\Omega_{\rm m}(1+z)^3 + (1-\Omega_{\rm m})(1+z)^{3(1+w_0+w_a)}e^{-3w_a z/(1+z)}\right]^{1/2}$	$\Omega_{\rm m}, w_0, w_a$

Table 1. Variations on the standard cosmological model that are tested in this paper, their Friedmann Equations, and the free parameters in the fit.

To compare data (Eq. 1) to theory we calculate the theoretical distance modulus, which is dependent on the set of cosmological parameters we are interested in (Θ, given in the right column of Table 1),

$$\mu(z,\Theta) = 5\log_{10}(D_{\rm L}(z,\Theta)/1\ {\rm Mpc}) + 25. \qquad (4)$$

We then take the difference between data and theory for every ith supernova, $\Delta\mu_i = \mu_{{\rm obs},i} - \mu(z_i,\Theta)$, and find the minimum of

$$\chi^2 = \Delta\mu_i \mathcal{C}^{-1}_{ij} \Delta\mu_j^T\ , \qquad (5)$$

where $\mathcal{C}^{-1}$ is the inverse covariance matrix (including both statistical and systematic errors) of the $\Delta\mu$ vector (see Sec. 3.6 of Vincenzi & The Dark Energy Survey 2024).

The uncertainty covariance matrix includes a diagonal statistical term (discussed Sec. 2.2) and a systematic term. The systematic covariance matrix is built following the approach in Conley et al. (2011) and accounts for systematics such as calibration, intrinsic scatter, and redshift corrections (see Table 6 of Vincenzi & The Dark Energy Survey 2024). Each element of the covariance matrix expresses the covariance between two of the SNe in the sample. The covariance matrix has dimensions of the number of supernovae $N_{\rm SNe} \times N_{\rm SNe}$ and we follow the formalism introduced by Brout et al. (2021) and Kessler et al. (2023).

Finally, we highlight that the absolute magnitude of SNe Ia and H_0 parameter (which appears in the luminosity distance) are completely degenerate and therefore combined in the single parameter $\mathcal{M} = M + 5\log_{10}(c/H_0)$, and all our results are marginalised over this term. Therefore, the value of H_0 has no impact on the fitting of our cosmological results, and we do not constrain H_0. While $\mathcal{M}$ has no impact on cosmology fitting, a precise value is needed to simulate bias corrections. The $\mathcal{M}$ uncertainty is below 0.01, resulting in a negligible impact on bias corrections (Brout et al. 2022a; Camilleri et al. in prep. 2024).

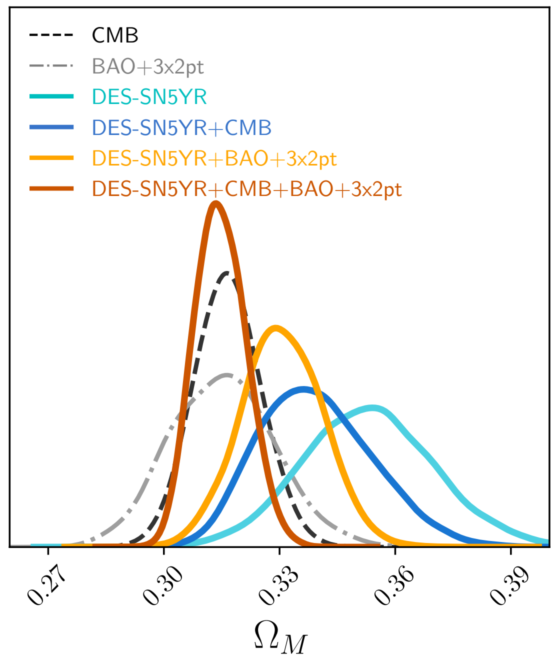

Figure 5. Constraints on matter density in the Flat-ΛCDM model from DES-SN5YR only (cyan), DES-SN5YR combined with CMB constraints from Planck Collaboration (2020) (blue), and DES-SN5YR combined with BAO+DES3×2pt (orange), and all probes combined (DES-SN5YR+BAO+DES3×2pt and CMB constraints, dark orange). CMB constraints only and BAO+3×2pt constraints alone are also shown for comparison (dashed and dotted-dashed respectively).

4. RESULTS

With the new DES high-redshift supernova sample we can put strong constraints on cosmological models. Of particular interest is whether dark energy is consistent with a cosmological constant or whether its density and/or equation of state parameter varies over the wide redshift range of our sample. The results of our cosmological fits are outlined in this section and summarised in Table 2, and their implications are explored in Sec. 5.

We estimate cosmological constraints using the CosmoSIS framework (Zuntz et al. 2015) and the samplers `emcee` for best fits (Foreman-Mackey et al. 2013) and

PolyChord for tension metrics (Handley et al. 2015),[5] except for fits that include BAO+DES3×2pt, which are calculated using PolyChord for both best fit and tensions.[6] For all fits we present the median of the marginalised posterior and cumulative 68.27% confidence intervals. The chains and code (with the flexibility to test other statistical choices) are available at https://github.com/des-science/DES-SN5YR. Figs. 5, 6, 7 and 8 all present the joint probability contours for 68.3% and 95.5%.

4.1. *Constraints on Cosmological Parameters*

4.1.1. *Flat-ΛCDM*

For the simplest parameterization, Flat-ΛCDM, $\Omega_{\rm m}$ is the only free parameter. We show the probability density function (PDF) of this constraint for DES-SN5YR in Figure 5; we measure a value of $\Omega_{\rm m} = 0.352 \pm 0.017$. We also show the probability distribution of the Planck Collaboration (2020) measurement of $\Omega_{\rm m}^{\rm Planck} = 0.317 \pm 0.008$. These are approximately 2σ apart, but not in significant tension as discussed in Sec 4.2.

Combining DES-SN5YR with Planck CMB gives $\Omega_{\rm m} = 0.338^{+0.016}_{-0.014}$, while combining with BAO+DES3×2pt gives $\Omega_{\rm m} = 0.330^{+0.011}_{-0.010}$. Combining all three gives $\Omega_{\rm m} = 0.315 \pm 0.007$. Interestingly, the combination of all data sets (dark orange in Fig. 5) gives a lower $\Omega_{\rm m}$ than any of the other combinations. The reason can be seen in Fig. 6, because the 'X marks the spot' point where all the contours cross the Flat Universe line is to the upper left of any contour alone.

4.1.2. *ΛCDM*

For ΛCDM, for DES-SN5YR we find $(\Omega_{\rm m}, \Omega_\Lambda) = (0.291^{+0.063}_{-0.065},\ 0.55 \pm 0.17)$, consistent with a flat universe ($\Omega_{\rm k} = 0.16 \pm 0.16$); see Fig. 6. Combining DES-SN5YR with BAO+DES3×2pt is also consistent with a flat Universe, with uncertainties on $\Omega_{\rm k}$ reduced to $\sim \pm 0.034$, while the combination with Planck gives $\Omega_{\rm k} = 0.010 \pm 0.005$. The combination of all three gives $\Omega_{\rm k} = 0.003^{+0.012}_{-0.013}$.

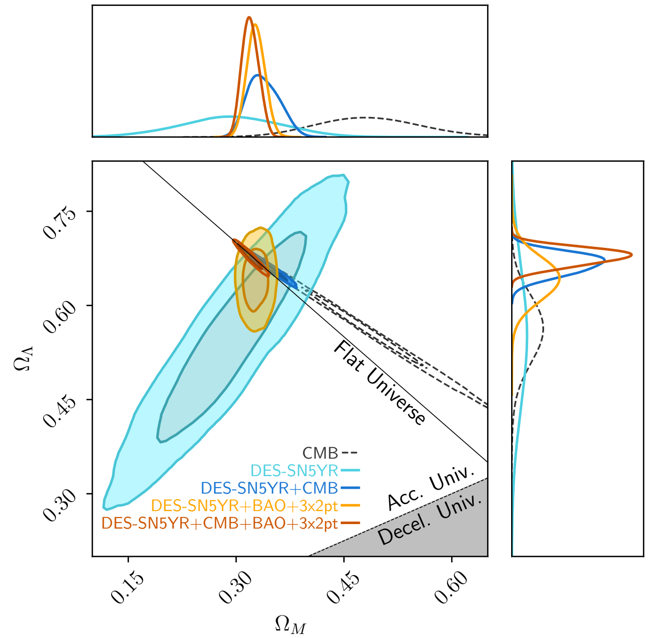

Figure 6. Constraints for ΛCDM model (curvature allowed) from the DES-SN5YR dataset only (cyan), from DES-SN5YR combined with BAO and weak lensing measurements (orange), and from DES-SN5YR combined with CMB measurements (blue). For comparison, we also present cosmological constraints from Planck Collaboration (2020) only (black dashed). The chains combining all probes are almost converged, but we are still running them a little longer.

4.1.3. *Flat-wCDM*

For Flat-wCDM, for DES-SN5YR we measure $(\Omega_{\rm m}, w) = (0.264^{+0.074}_{-0.096}, -0.80^{+0.14}_{-0.16})$; see Fig. 7. This is consistent with a cosmological constant (within 2σ), although our data favor values for w slightly larger than -1.

The $w - \Omega_{\rm m}$ contours from SN alone are highly non-Gaussian with a curved 'banana'-shaped degeneracy. That means it is inefficient to cite a best-fit value for w or $\Omega_{\rm m}$ alone, as a small shift along the degeneracy direction can result in large shifts in the best-fit values. To solve this problem, in Camilleri et al. (in prep. 2024) we introduce a new parameter, $Q_H(z) \equiv -\ddot{a}/(aH_0^2) \equiv q(H/H_0)^2$. This combination of the deceleration parameter q and the Friedmann equation H/H_0 follows the curve of the degeneracy in the $w - \Omega_{\rm m}$ plane. Therefore, measuring $Q_H(z)$ summarises the supernova information in a single, almost degeneracy-free value.[7] One has

[5] For each `emcee` fit we use a number of walkers that is at least twice the number of parameters and ensure the number of samples in the chain is greater than 50 times the autocorrelation function, τ ($N_{\rm samples}/\tau > 50$). For each PolyChord fit, we use a minimum of 60 live points, 30 repeats, and an evidence tolerance requirement of 0.1. When combining with other datasets we run simultanous MCMC chains including all relevant data vectors. Flat priors that encapsulate at least the 99.7% confidence region were chosen in each case.

[6] The main advantage of `emcee` is it gives slightly more accurate best fit χ^2 than PolyChord. However, we decided the tiny improvement in accuracy was not worth the environmental impact (Stevens et al. 2020) of the extra compute time (which was substantial for the many-dataset fits).

[7] Similar to the S_8 parameter used in lensing studies to approximate σ_8-$\Omega_{\rm m}$ constraints.

Table 2. Results for four different cosmological models, sorted into sections for different combinations of observational constraints. These are the medians of the marginalised posterior with 68.27% integrated uncertainties ('cumulative' option in ChainConsumer). For each fit we also show the χ^2 per degree of freedom as a measure of the goodness of fit.

	Ω_m	Ω_k	w_0	w_a	χ^2/dof
DES-SN5YR (no external priors)					
Flat-ΛCDM	0.352 ± 0.017	-	-	-	1649.2/1734=0.951
ΛCDM	$0.291^{+0.063}_{-0.065}$	0.16 ± 0.16	-	-	1648.3/1733=0.951
Flat-wCDM	$0.264^{+0.074}_{-0.096}$	-	$-0.80^{+0.14}_{-0.16}$	-	1647.7/1733=0.951
Flat-w_0w_aCDM	$0.495^{+0.033}_{-0.043}$	-	$-0.36^{+0.36}_{-0.30}$	$-8.8^{+3.7}_{-4.5}$	1641.1/1732=0.948
DES-SN5YR + Planck 2020					
Flat-ΛCDM	$0.338^{+0.016}_{-0.014}$	-	-	-	2236.7/2349=0.952
ΛCDM	$0.359^{+0.014}_{-0.016}$	0.010 ± 0.005	-	-	2230.5/2348=0.950
Flat-wCDM	$0.337^{+0.013}_{-0.011}$	-	$-0.955^{+0.032}_{-0.037}$	-	2233.5/2348=0.951
Flat-w_0w_aCDM	$0.325^{+0.016}_{-0.012}$	-	-0.73 ± 0.11	$-1.17^{+0.55}_{-0.62}$	2230.9/2347=0.951
DES-SN5YR + SDSS BAO and DES Y3 3×2pt					
Flat-ΛCDM	$0.330^{+0.011}_{-0.010}$	-	-	-	2194/2212=0.992
ΛCDM	$0.327^{+0.012}_{-0.011}$	0.030 ± 0.034	-	-	2194/2211=0.992
Flat-wCDM	$0.323^{+0.011}_{-0.010}$	-	$-0.922^{+0.035}_{-0.037}$	-	2188/2211=0.989
Flat-w_0w_aCDM	0.334 ± 0.012	-	$-0.778^{+0.088}_{-0.080}$	$-0.93^{+0.46}_{-0.53}$	2191/2210=0.992
DES-SN5YR + Planck 2020 + SDSS BAO and DES Y3 3×2pt					
Flat-ΛCDM	0.315 ± 0.007	-	-	-	2791/2828=0.987
ΛCDM	$0.327^{+0.026}_{-0.032}$	$0.003^{+0.012}_{-0.013}$	-	-	3210/2827=1.157
Flat-wCDM	0.321 ± 0.007	-	-0.941 ± 0.026	-	2785/2827=0.985
Flat-w_0w_aCDM	0.325 ± 0.008	-	$-0.773^{+0.075}_{-0.067}$	$-0.83^{+0.33}_{-0.42}$	2782/2826=0.984

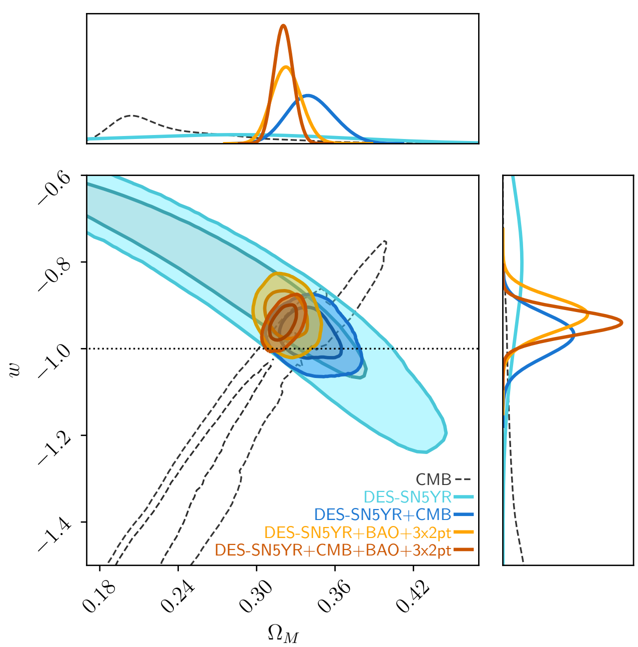

Figure 7. Same as Fig. 6 but for Flat wCDM model. The horizontal dotted line marks the equation of state values for a cosmological constant, i.e. $w = -1$.

to choose the redshift at which one quotes $Q_H(z)$, to best match the angle of the degeneracy for the redshift range of the sample. We find $Q_H(z = 0.2) = -0.340 \pm 0.032$ using DES-SN5YR only (see Camilleri et al. in prep. 2024, for more details). This can be used to roughly approximate the DES-SN5YR results without the need for a full fit to the Hubble diagram.

The degeneracy in the $w - \Omega_\mathrm{m}$ plane is broken when combining SNe with external probes. When combining with Planck, we measure $(\Omega_\mathrm{m}, w) = (0.337^{+0.013}_{-0.011}, -0.955^{+0.032}_{-0.037})$, again within 2σ of a cosmological constant. Planck alone provides only a loose constraint on the equation of state parameter of dark energy, $w^{\mathrm{Planck}} = -1.51^{+0.27}_{-0.18}$; combining with DES-SN5YR reduces the uncertainty significantly due to the different degeneracy direction, demonstrating the combined constraining power of these two complementary probes.

When combining DES-SN5YR with BAO+DES3×2pt we find $w = -0.922^{+0.035}_{-0.037}$, slightly over 2σ from the cosmological constant. This data combination demonstrates that these late-universe probes alone provide constraints that are consistent with – and of comparable constraining power to – the combination of SN and CMB data. The full combination of all data sets gives $w = -0.941 \pm 0.026$.

4.1.4. *Flat-w_0w_aCDM*

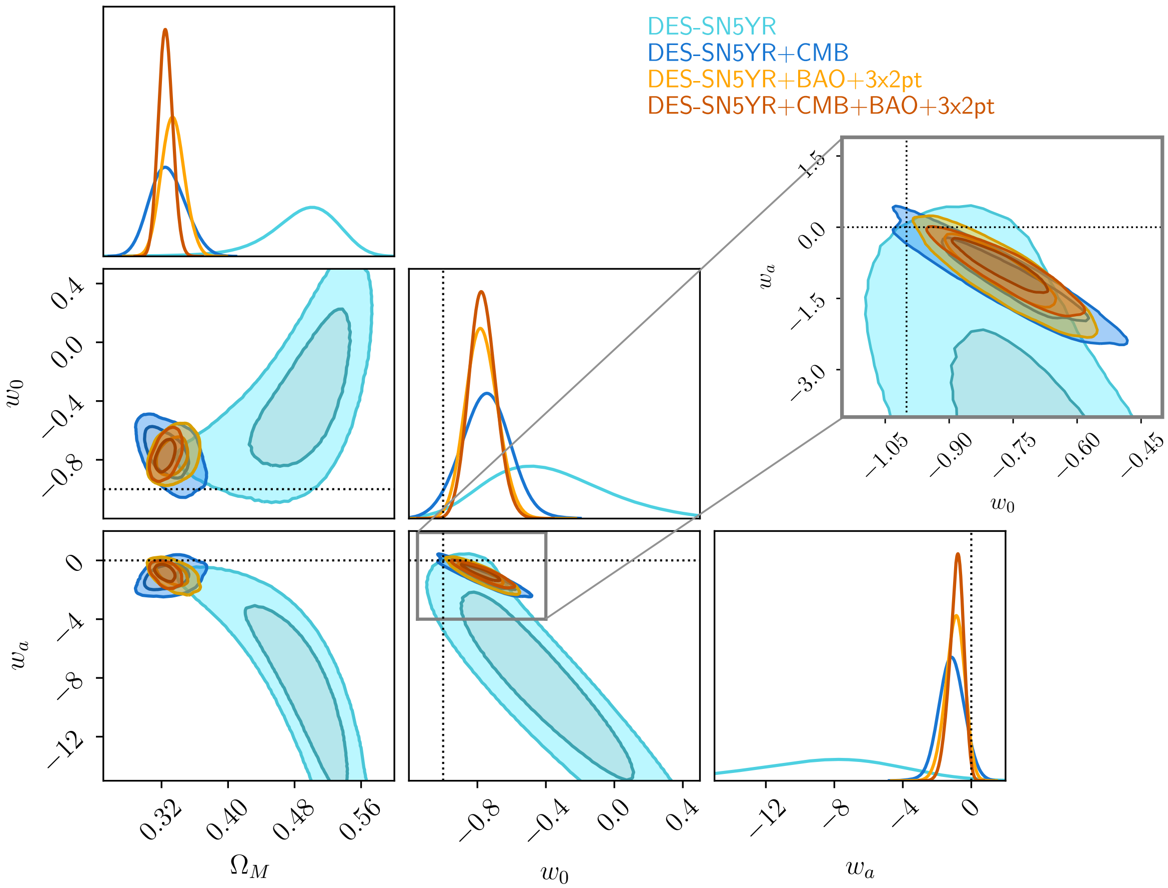

Figure 8. Same as Fig. 6 but for $w_0 w_a$CDM model. The dashed crosshairs mark the equation of state values for a cosmological constant, i.e. $(w_0, w_a) = (-1, 0)$. The residuals between the DES-SN5YR best fit Flat-$w_0 w_a$CDM w.r.t. Flat-wCDM model are presented in Fig. 4.

The best-fit Flat-$w_0 w_a$CDM model from DES-SN5YR alone is slightly over 2σ from a cosmological constant, marginally preferring a time-varying dark energy $(\Omega_{\rm m}, w_0, w_a)$ $=(0.495^{+0.033}_{-0.043},\ -0.36^{+0.36}_{-0.30},\ -8.8^{+3.7}_{-4.5})$; see Fig. 8.

When combining DES-SN5YR and the CMB, we find $(\Omega_{\rm m}, w_0, w_a)$ $=(0.325^{+0.016}_{-0.012}, -0.73 \pm 0.11, -1.17^{+0.55}_{-0.62})$, which again deviates slightly from the cosmological constant. The same trend is seen when combining with BAO+DES3×2pt and with all data combined. The negative w_a means the dark energy equation of state parameter is *increasing* with time (sometimes referred to as a "thawing" model).

4.2. *Goodness of fit and tension*

4.2.1. χ^2 *per degree of freedom*

To assess whether our best fits are good fits we calculate the χ^2 per degree of freedom for all our dataset and model combinations; see the last column of Table 2.

The χ^2 we use for this test is the maximum likelihood of the entire parameter space, not the marginalised best fit for each parameter.

The number of degrees of freedom is the number of data points minus the number of parameters that are common to all datasets (i.e., the cosmological parameters of interest). The number of data points added by the CMB, BAO, and DES3×2pt is respectively 615, 8, and 471. Due to our treatment of contamination (by inflating the uncertainties of SNe with a low $P_{\rm Ia}$), we approximate the *effective* number of data points in the DES-SN5YR sample by $\sum P_{\rm B(Ia)} = 1735$ (rather than the total number of data points, 1829).

A good fit should have χ^2/d.o.f.$\sim$ 1.0. The slightly low χ^2/d.o.f. for the DES-SN5YR data arises because $\sum P_{\rm B(Ia)}$ only approximates the number of degrees of freedom, and the same behaviour is also seen in simulations.

4.2.2. *Suspiciousness*

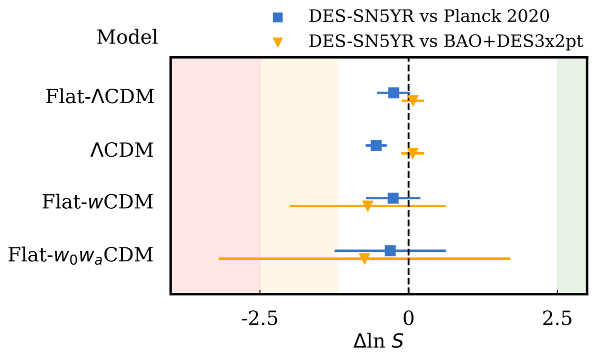

Figure 9. Measurements of Suspiciousness between the DES-SN5YR and Planck 2020 datasets for the four models constrained in this paper. The further to the left indicates higher tension where the shaded regions reflect "substantial" (yellow) and "strong" (red) evidence of tension according to Jeffreys' scale (Jeffreys 1961). The values and uncertainties represent the mean and standard deviation of realizations estimating sample variance using the ANESTHETIC software.

Suspiciousness (Handley & Lemos 2019) is closely related to the Bayes ratio, R,[8] and can be used to assess whether different datasets are consistent. However, while the Bayes ratio has been shown to be prior-dependent (Handley & Lemos 2019), with wider prior widths boosting the confidence, Suspiciousness is prior independent. Therefore, Suspiciousness is ideal for cases such as ours where we have chosen deliberately wide and uninformative priors (Lemos et al. 2021, Sec. 4.2). Jeffreys' scale (Jeffreys 1961) suggests $\ln S < -2.5$ is "strong" tension, $-2.5 < \ln\ S < -1.2$ is "substantial" tension, and $\ln S > -1.2$ indicates the datasets are in agreement.

We determine $\ln S$ using the ANESTHETIC software (Handley 2019), which produces an ensemble of realizations used to estimate sample variance. Results are then quoted using the mean of the ensemble, with the error bars reflecting the standard deviation.

In Fig. 9 we plot the Suspiciousness values for the DES-SN5YR data *vs* Planck 2020 and *vs* BAO+DES3×2pt data. We find no indication of tension for the four models investigated in this paper.

4.3. *Model Selection*

Finally, we use Bayesian Evidence to test whether the extra parameters in the more complex models we test are warranted, given the data. In Fig. 10, we present the difference in the logarithm of the Bayesian Evidence, $\Delta(\ln BE)$, relative to Flat-ΛCDM for the four different models tested in this analysis and for the three combinations of datasets used in Fig. 10.

[8] Suspiciousness, S, is related to the Bayes ratio R and Bayesian information I and is defined as $\ln S = \ln R - \ln I$.

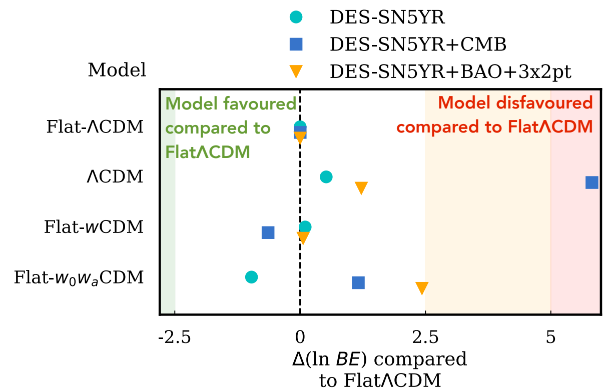

Figure 10. Bayesian Evidence difference relative to Flat-ΛCDM ($\Delta(\ln BE)$). We present the results for the four different models tested in this analysis and for the three combination of datasets used (DES only in cyan, DES+Planck in blue, DES+BAO+DES3×2pt in orange). An increase (decrease) in $\Delta(\ln BE)$ indicates that a model is disfavoured (favoured) compared to Flat-ΛCDM.

To evaluate the strength of evidence when comparing Flat-ΛCDM with more complex models, we again use Jeffreys' scale. This empirical scale suggests that $\Delta(\ln BE) > 2.5$ (and < -2.5) is moderate evidence against (in support of) the more complex model, whereas $\Delta(\ln BE) > 5$ (and < -5) is strong evidence against (in support of) the more complex model (for a review of model selection in cosmology see Trotta 2008). We note that none of the datasets considered in this analysis strongly favours cosmological models beyond Flat-ΛCDM. The priors that we choose for model comparison are $w \in (-1.5, -0.5)$, $w_a \in (-10, 10)$ and $\Omega_k \in (-0.5, 0.5)$. We consider these priors (which determine the penalty for more complex models) to be reasonable in terms of general considerations, such as avoiding universes that are younger than generally accepted stellar ages (see Section 5.1.3). We also find the results to be consistent with the Akaike Information Criteria, another commonly used model comparator.

5. DISCUSSION

5.1. *The big questions*

5.1.1. *Is the expansion of the Universe accelerating?*

Twenty five years ago Riess et al. (1998) found 99.5%–99.9% (2.8σ to 3.9σ) evidence for an accelerating Universe, by considering the deceleration parameter $q \equiv (a\ddot{a})\dot{a}^{-2}$ and integrating over the likelihood that $q_0 < 0$. Importantly they note that since q_0 is measured at the present day but the data span a wide range of redshifts, q_0 can only be measured within the context of a model, either cosmographic or physically motivated. They used the ΛCDM model, in which $q_0 = \Omega_\mathrm{m}/2 - \Omega_\Lambda$.

Doing the same with DES-SN5YR data gives 99.99998% confidence (5.2σ) that $q_0 < 0$ in ΛCDM, or a 2×10^{-7} chance that the expansion of the Universe is *not* accelerating. As noted in Section 4.1.3, our confidence is even higher that the universe *was* accelerating at $z \sim 0.2$. When we further assume flatness, the confidence in an accelerating Universe is overwhelming (no measurable likelihood for a decelerating Universe) and we find $q_0 = -0.530^{+0.018}_{-0.017}$. For more fits of q_0 using a cosmographic approach see Camilleri et al. (in prep. 2024).

5.1.2. *Is dark energy a cosmological constant?*

As seen in Sec 4.1, a cosmological constant is a good fit to our data, but not the best fit. Our best fit equation of state parameter is slightly (more than 1σ) higher than the cosmological constant value of $w = -1$ (both for SNe alone and in combination with Planck or BAO+DES3×2pt). This agrees with the recent result from the UNION3 compilation analyzed with the UNITY framework (Rubin et al. 2023). Pantheon+ (Brout et al. 2022a) results were within 1σ of $w = -1$, but also on the high side ($w = -0.90 \pm 0.14$).

Furthermore, our analysis slightly prefers a time-varying dark energy equation of state parameter when we fit for $w(a)$ such that the equation of state parameter increases with time (again for all data combinations), known as a "thawing" model. Model selection, however, is inconclusive.

The constraints on time-varying w are enabled by the wide redshift range of the DES-SN5YR sample. Our analysis as described in Vincenzi & The Dark Energy Survey (2024) gives us confidence that systematic uncertainties in this data are below the level of our statistical precision. Nevertheless, it is important to recognise that (a) the low-z sample is the one for which we still have the least systematic control and (b) the very high-redshift SNe are the ones for which bias-corrections are large (> 0.1 mag) and more uncertain (e.g., accurate estimation of spectroscopic redshift efficiency is more challenging as we go to higher redshifts), and for which the uncertainties on the rest-frame UV part of the SN Ia spectral energy distribution have more impact on SN distances estimations (see also Brout et al. 2022a).

To test whether our fits were being dominated by any particular redshift range we ran cosmological fits (a) removing low-z data (i.e., DES SNe alone) and (b) removing high-z data (i.e. removing ~ 80 SNe at $z > 0.85$, which we have only measured in two bands; see Fig. 2). Most of the cosmological results obtained with the sub-samples are consistent with the results found for the full sample. However, we found that removing the low-z sample shifts the contours in the Flat-wCDM slightly down, which would make the combined fits more consistent with $w = -1$. The Flat-w_0w_aCDM results are stable to sub-sample selection.

We showed in Vincenzi & The Dark Energy Survey (2024) that systematic uncertainties are sub-dominant to the statistical uncertainties in our sample. Nevertheless, in the future a new low-redshift sample (see Sec. 5.3) would help alleviate any remaining doubt about calibration and systematics in the existing low-z sample, and an even higher-redshift supernova survey would help alleviate any modelling concerns by minimizing selection effects even at $z \sim 1$.

5.1.3. *How old is the Universe?*

One of the issues that the discovery of dark energy solved is the age of the Universe (t_0) problem – globular cluster age estimates, in combination with high estimates of H_0, were inconsistent with models that were not accelerating (VandenBerg et al. 1996; Gratton et al. 1997; Chaboyer et al. 1998).

Our results, which favor a dark energy equation of state parameter slightly higher than $w = -1$ would imply that the age is slightly *younger* than the age found in a Universe where dark energy is a cosmological constant (for the same values of H_0 and present dark energy density).

To calculate the Universe's age, one needs a value of H_0 in addition to the best fit cosmological model. Since we do not constrain H_0 in this analysis, we present our measurement of the combination H_0t_0. In other words, we give t_0 in units of the Hubble time $t_H \equiv 1/H_0$.[9] Our

[9] If $H_0 = 68\ \mathrm{km\,s^{-1}Mpc^{-1}}$, $t_H(68) = 14.38$ Gyr.
If $H_0 = 73\ \mathrm{km\,s^{-1}Mpc^{-1}}$, $t_H(73) = 13.40$ Gyr.

best-fit DES-SN5YR result in Flat-ΛCDM would have an age of $(0.921 \pm 0.013)t_H$. This is $\sim 3\%$ younger than Planck ($t_{\rm age}^{\rm Planck} = (0.950 \pm 0.007)t_H$), corresponding to an age difference of approximately -0.4 Gyr. Our best fit Flat-w_0w_aCDM model gives an age $(0.86 \pm 0.02)t_H$, about 9% younger than the Flat-ΛCDM Planck result, corresponding to an age difference of approximately -1.3 Gyr. Such a young age is unlikely given the age of the oldest globular clusters (Valcin et al. 2020; Cimatti & Moresco 2023; Ying et al. 2023). In the future this could be used as a prior to limit the feasible range of time-varying dark energy.

5.1.4. *Does our best fit resolve the Hubble tension?*

As pointed out in Planck Collaboration (2020, their Sec. 5.4), the only basic extensions to the base Flat-ΛCDM model that resolve the H_0 tension are those in which the dark energy equation of state is allowed to vary away from $w = -1$. In the wCDM model a phantom equation of state parameter of $w \sim -1.5$ would help resolve the tension (Di Valentino et al. 2021, their Sec. 5.1), and it is clear from Fig. 7 that CMB alone actually prefers $w < -1$. (In this model Planck alone does not constrain H_0 very tightly, and they refrain from quoting a value, see Table 5 of Planck Collaboration (2020), but lower w correlates with higher H_0.) However, the DES-SN5YR data shows a slight tendency for $w > -1$, essentially ruling out this solution within wCDM.

5.2. *Comparison with DES-SN3YR and Pantheon+*

It is informative to compare the results of the DES-SN3YR analysis (Dark Energy Survey Collaboration 2019; Brout et al. 2019a) with the results of the DES-SN5YR analysis presented in this work. The DES-SN3YR analysis included 207 *spectroscopically confirmed* SNe Ia from DES and 127 low-redshift SNe from CfA and CSP samples (see also Fig. 3). A fraction of those events is in common between both analyses (55 from low-z external samples and 146 DES SNe).[10]

However, the DES-SN3YR analysis differs from the analysis presented here in many aspects. The SN Ia intrinsic scatter modelling has been significantly improved

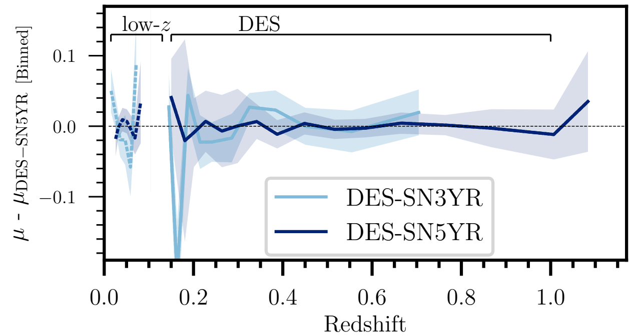

Figure 11. Comparison between Hubble residuals for the DES-SN3YR and DES-SN5YR analyses w.r.t. the best fit Flat-wCDM for the DES-SN5YR analysis. Hubble residuals are binned in redshift and we present the weighted mean and standard deviation of the mean in each redshift bin. The redshift range covered by the low-z sample is highlighted and shown with thick dotted lines. The two DES samples are consistent with each other. Note the DES-SN3YR analysis only includes spectroscopically confirmed SNe whereas the DES sample in the DES-SN5YR analysis consists entirely of photometrically identified SNe Ia and extends to higher-z.

(from 'G10' and constant $\sigma_{\rm int}$ floor, to the more sophisticated modelling of intrinsic scatter introduced by Brout & Scolnic 2021; Popovic et al. 2023a), the BBC software has been updated (from BBC '5D' and a binned approach, to BBC '4D' and an unbinned approach), the $x_1 - M_\star$ correlations have been incorporated into simulations (following the work by Smith et al. 2020b; Popovic et al. 2021), and the light-curve fitting model has been updated from the SALT2 model to the SALT3 model (see Taylor et al. 2023, for a comparison between SALT2 and SALT3 using the DES-SN3YR sample). Finally, the DES-SN3YR analysis did not require machine-learning classification and the implementation of the BEAMS approach because it is a sample of spectroscopically selected SNe Ia. We compare the final SN distances in Fig. 11 and find consistent results (differences in binned distances are on average 0.02 mag, even in the redshift ranges where contamination is expected to be high). The cosmological results from DES-SN3YR and DES-SN5YR are fully consistent within uncertainties (when assuming Flat-ΛCDM, Ω_M are 0.331 ± 0.038 and 0.352 ± 0.017 for DES-SN3YR and DES-SN5YR respectively, while when assuming Flat-wCDM and including CMB priors, w are -0.978 ± 0.059 and $-0.955^{+0.032}_{-0.037}$).

The other main dataset we can compare to is Pantheon+, which contains a significant amount of independent data (all the high-z data). The DES sample is on average much higher redshift than the Pantheon+ sample (see Fig. 3), with over a quarter of the DES-SN5YR sample being at high enough redshift ($z \gtrsim 0.64$) to probe

[10] Not all events included in the DES-SN3YR analysis are included in the DES-SN5YR analysis and vice-versa. This is due to the two analyses implementing different sample cuts. For example the $z > 0.025$ cut and the requirement for a host-galaxy redshift in DES-SN5YR exclude respectively 44 and 29 low-z SNe that were in the DES-SN3YR sample. DES-SN5YR also uses a new SALT model (which affects the SALT-based cuts), and is restricted to SNe that pass selection cuts across all systematic tests (see Table 4 in Vincenzi & The Dark Energy Survey 2024).

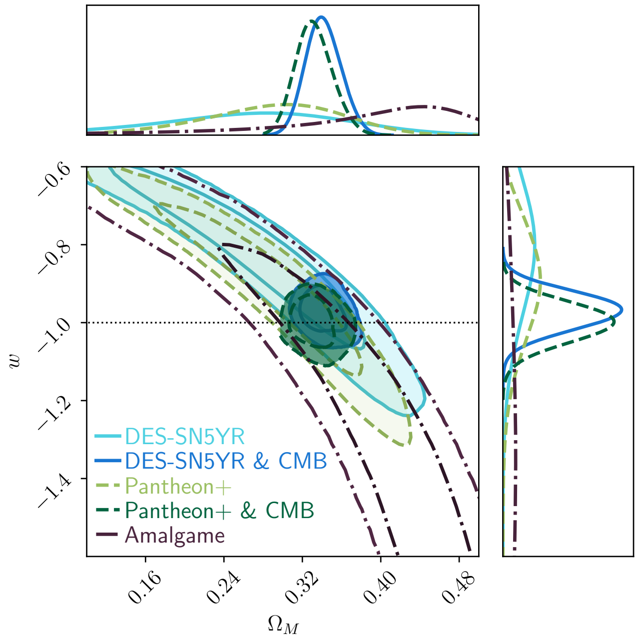

Figure 12. Constraints in Flat-wCDM from the DES-SN5YR sample, the Pantheon+ sample (with and without CMB priors), and the Amalgame sample. The constraining power of the DES-SN5YR and Pantheon+ samples is comparable and consistent, despite Pantheon+ being a spectroscopic SN Ia sample combining 17 different surveys. The 'Amalgame' sample includes the SDSS and PS1 photometric SN samples ($>$ 1700 intermediate-redshift and high-redshift SNe), however it does not include a low-z anchoring sample (hence the larger contours). DES-SN5YR and Pantheon+ are also combined with CMB constraints (for both we use the Planck lite Python implementation presented by Prince & Dunkley 2019). The horizontal dotted line marks the equation of state values for a cosmological constant.

the likely *decelerating*[11] period of the Universe (compared to 6% in Pantheon+). We show a comparison of the contours in Fig. 12. We find very similar constraining power between Pantheon+ and DES-SN5YR, and the DES-SN5YR value of w is within 1σ of Pantheon+ (Brout et al. 2022a). These analyses are not fully independent as a fraction of the low-z sample is shared. However, all of the high-z dataset is independent, and DES is a photometric sample while Pantheon+ is fully spectroscopic. The constraints on w are similar between DES and Pantheon+ as DES high-z has better precision per SN than Pantheon+ and has significantly higher statistical power at $z > 0.4$ (see Fig. 3), but Pantheon+ used 2× more low-redshift SNe (which we do not include in order to be able to better control systematic uncertainties).

5.3. *DES and Next Generation Supernova Samples*

This analysis has shown that moving from a spectroscopically confirmed sample as done in Dark Energy Survey Collaboration (2019) to a photometric sample can increase the sample size of well-measured supernovae significantly (from 207 DES SNe Ia in DES-SN3YR to $>$ 1600 in DES-5YR), consistent with an analysis of Pan-STARRS SNe in Jones et al. (2018). This improvement arises because photometric classification alleviates the bottleneck of limited spectroscopic resources. The improvement will increase for future surveys as more candidates are discovered, but the available time for spectroscopy does not increase commensurately. Importantly, the work of Vincenzi & The Dark Energy Survey (2024) shows that systematic uncertainties due to photometric classification are not limiting. Instead, the 'conventional' systematics of calibration and modeling the intrinsic scatter remain the most significant challenges.

There is potential for further increase of the statistical power of the DES sample if one moves to using SNe in which a host galaxy spectroscopic redshift was not acquired and instead relies on photometric redshifts of the SNe and the galaxy. This path was explored by Chen et al. (2022) for a subset of DES SNe, namely ones that occur in redMaGiC galaxies, and has been explored as well for SuperNova Legacy Survey (SNLS, Ruhlmann-Kleider et al. 2022) and the Vera C. Rubin Observatory Legacy Survey of Space and Time (LSST) in Mitra et al. (2023). These analyses show that the use of photo-zs do not introduce systematic uncertainties to a scale similar to the statistical uncertainties. This potential is highlighted by the ≈ 2400 SNe Ia identified without host galaxy spectroscopic redshift in DES that could be used for this type of analysis (Möller & the DES Collaboration in prep. 2024).

The DES supernova survey was supported by the 6-year OzDES survey on the Anglo-Australian Telescope (described in Lidman et al. 2020), which took multi-fibre observations of host galaxies to acquire redshifts of host galaxies of SNe. The total investment of this program was 100 nights, and for roughly 75% of the targeted host galaxies a spectroscopic redshift has been secured. This program was fortuitous as the cameras for OzDES and DECam have a nearly identical field-of-view. It would be difficult to imagine the resources needed to reproduce this joint program for LSST, which will find millions of SNe across 18,000 square degrees (Ivezić et al. 2019; Sánchez et al. 2022) (compared to the 27 square degrees of DES SNe).

[11] The redshift the redshift at which the Universe began accelerating in ΛCDM is $z_{\rm acc} = (2\Omega_\Lambda/\Omega_{\rm m})^{1/3} - 1$.

As statistical precision continues to improve thanks to the increased number of supernovae, a main theme for systematic analysis is second-order relations between different systematics. Typically, systematics are treated independently when building the covariance matrix. We have implemented a method to account for calibration systematics along with light-curve model systematics together, but this is currently the only joint exercise. This type of work will grow in importance. For example, while photometric classification does not directly cause a large increase in the error budget, it hinders the ability to constrain the intrinsic scatter model preferred by the data. Potentially, if LSST and other surveys such as those enabled by the Nancy Grace Roman Space Telescope have enough supernovae (Rose et al. 2021), the dataset will be large enough to enable a forward modeling approach such as the Approximate Bayesian Computation method introduced in Jennings et al. (2016) and worked on in Armstrong et al. (in prep), which could vary all systematics, nuisance, and cosmological parameters at the same time to compare against the data.

Furthermore, as discussed in Section 5.1.2, modeling of the low-z sample remains a source of systematic uncertainty. This sample comes from a multitude of surveys, even though we have removed many of the older inhomogeneous sources compared to analyses like Pantheon+. In the near future, we expect additions from Zwicky Transient Factory (Smith et al. in prep. 2024), Young Supernova Experiment (Jones et al. 2021; Aleo et al. 2023), and Dark Energy Bedrock All-sky Supernova Survey (DEBASS, PI: Brout) to improve low-z constraints of the SN Hubble Diagram, given their improved calibration and better understood selection function.[12] DEBASS will be particularly fruitful as it is a low-redshift sample taken with DECam, so a single calibration will be used for the full sample of DEBASS+DES, similar to the work for PS1 in Jones et al. (2019). Using simulations, we estimate that quadrupling the size of our low-z sample (from ~ 200 to ~ 800 SNe expected from this next generation of low-z SN surveys) could allow us to reduce uncertainties on w by ~ 30 per cent (for a Flat$w$CDM model, using SN data alone).

Lastly, we note that while LSST and Roman may help improve a number of these issues, the first data release is still > 3 years away. We encourage work with the DES-SN sample as presented here, combined with other samples, including the UNION3 compilation (Rubin et al. 2023), which appeared while this paper was under internal review. Popovic et al. (2023b) recently showed the ability to combine separate photometric samples (PS1 and SDSS) into the Amalgame sample (also shown in Fig. 12, and a similar analysis can be done by combining DES with these. It is reasonable to expect that with new low-redshift samples, and combination of high-redshift photometric samples, a sample with > 5000 likely SNe Ia can be compiled in the very near future.

[12] These upcoming low-z surveys are magnitude-limited rather than targeted, therefore they provide SN samples with a well defined selection function.

6. CONCLUSIONS

The DES Supernova survey stands as a groundbreaking milestone in SN cosmology. With a single survey, we effectively tripled the number of observed SNe Ia at $z > 0.2$ and quintupled the number beyond $z > 0.5$. Here we present the unblinded cosmological results, and in companion papers make public the calibrated light curves and Hubble diagram from the full sample of DES Type Ia supernovae (Sánchez in prep. 2024; Vincenzi & The Dark Energy Survey 2024).

After combining the 1635 DES SNe (of which 1499 have a probability > 0.5 of being a SN Ia) with 194 existing low-z SNe Ia we present final cosmological results for four variants on ΛCDM cosmology, as summarised in Table 2.

The standard Flat-ΛCDM cosmological model is a good fit to our data. When fitting DES-SN5YR alone and allowing for a time-varying dark energy we do see a slight preference for a dark energy equation of state that becomes more positive with time ($w_a < 0$) but this is only at the $\sim 2\sigma$ level, and Bayesian Evidence ratios do not strongly prefer the Flat-w_0w_aCDM cosmology.

We find differences with the cosmological results from the CMB as measured by Planck Collaboration (2020), but are consistent within $\sim 2\sigma$ in all models tested and the Suspiciousness statistic indicates that these datasets are in agreement.

Critically, the DES-SN5YR analysis shown here demonstrates that contamination due to SN classification and host-galaxy matching is not a limiting systematic for SN cosmology; this opens the path for a new era of cosmological measurements using SN samples that are not limited by live spectroscopic follow-up of SNe. Instead, our analysis shows the SN community that there are other factors that will be crucial for the success of future SN experiments: the necessity for a high-quality low-redshift sample, the necessity for a robust UV and NIR extension of light-curve fitting models, the necessity for an excellent control of selection effects both across the entire redshift range, and the necessity for an improvement in our understanding of SN Ia intrinsic scatter properties and the role played by interstellar dust.

Future work will conclude the Dark Energy Survey by combining these supernova results with the other three pillars of DES cosmology, namely baryon acoustic oscillations, galaxy clustering, and weak lensing.

ACKNOWLEDGMENTS

T.M.D., A.C., R.C., S.H., acknowledge the support of an Australian Research Council Australian Laureate Fellowship (FL180100168) funded by the Australian Government. M.S., H.Q., and J.L are supported by DOE grant DE-FOA-0002424 and NSF grant AST-2108094. R.K. is supported by DOE grant DE-SC0009924. M.V. was partly supported by NASA through the NASA Hubble Fellowship grant HST-HF2-51546.001-A awarded by the Space Telescope Science Institute, which is operated by the Association of Universities for Research in Astronomy, Incorporated, under NASA contract NAS5-26555. LK thanks the UKRI Future Leaders Fellowship for support through the grant MR/T01881X/1. L.G. acknowledges financial support from the Spanish Ministerio de Ciencia e Innovación (MCIN), the Agencia Estatal de Investigación (AEI) 10.13039/501100011033, and the European Social Fund (ESF) "Investing in your future" under the 2019 Ramón y Cajal program RYC2019-027683-I and the PID2020-115253GA-I00 HOSTFLOWS project, from Centro Superior de Investigaciones Científicas (CSIC) under the PIE project 20215AT016, and the program Unidad de Excelencia María de Maeztu CEX2020-001058-M, and from the Departament de Recerca i Universitats de la Generalitat de Catalunya through the 2021-SGR-01270 grant. We acknowledge the University of Chicago's Research Computing Center for their support of this work. A.M. is supported by the ARC Discovery Early Career Researcher Award (DECRA) project number DE230100055.

Funding for the DES Projects has been provided by the U.S. Department of Energy, the U.S. National Science Foundation, the Ministry of Science and Education of Spain, the Science and Technology Facilities Council of the United Kingdom, the Higher Education Funding Council for England, the National Center for Supercomputing Applications at the University of Illinois at Urbana-Champaign, the Kavli Institute of Cosmological Physics at the University of Chicago, the Center for Cosmology and Astro-Particle Physics at the Ohio State University, the Mitchell Institute for Fundamental Physics and Astronomy at Texas A&M University, Financiadora de Estudos e Projetos, Fundação Carlos Chagas Filho de Amparo à Pesquisa do Estado do Rio de Janeiro, Conselho Nacional de Desenvolvimento Científico e Tecnológico and the Ministério da Ciência, Tecnologia e Inovação, the Deutsche Forschungsgemeinschaft and the Collaborating Institutions in the Dark Energy Survey.

The Collaborating Institutions are Argonne National Laboratory, the University of California at Santa Cruz, the University of Cambridge, Centro de Investigaciones Energéticas, Medioambientales y Tecnológicas-Madrid, the University of Chicago, University College London, the DES-Brazil Consortium, the University of Edinburgh, the Eidgenössische Technische Hochschule (ETH) Zürich, Fermi National Accelerator Laboratory, the University of Illinois at Urbana-Champaign, the Institut de Ciències de l'Espai (IEEC/CSIC), the Institut de Física d'Altes Energies, Lawrence Berkeley National Laboratory, the Ludwig-Maximilians Universität München and the associated Excellence Cluster Universe, the University of Michigan, NSF's NOIRLab, the University of Nottingham, The Ohio State University, the University of Pennsylvania, the University of Portsmouth, SLAC National Accelerator Laboratory, Stanford University, the University of Sussex, Texas A&M University, and the OzDES Membership Consortium.

Based in part on observations at Cerro Tololo Inter-American Observatory at NSF's NOIRLab (NOIRLab Prop. ID 2012B-0001; PI: J. Frieman), which is managed by the Association of Universities for Research in Astronomy (AURA) under a cooperative agreement with the National Science Foundation. Based in part on data acquired at the Anglo-Australian Telescope. We acknowledge the traditional custodians of the land on which the AAT stands, the Gamilaraay people, and pay our respects to elders past and present. Parts of this research were supported by the Australian Research Council, through project numbers CE110001020, FL180100168 and DE230100055.

The DES data management system is supported by the National Science Foundation under Grant Numbers AST-1138766 and AST-1536171. The DES participants from Spanish institutions are partially supported by MICINN under grants ESP2017-89838, PGC2018-094773, PGC2018-102021, SEV-2016-0588, SEV-2016-0597, and MDM-2015-0509, some of which include ERDF funds from the European Union. IFAE is partially funded by the CERCA program of the Generalitat de Catalunya. Research leading to these results has received funding from the European Research Council under the European Union's Seventh Framework Program (FP7/2007-2013) including ERC grant agreements 240672, 291329, and 306478. We acknowledge support from the Brazilian Instituto Nacional de

Ciência e Tecnologia (INCT) do e-Universo (CNPq grant 465376/2014-2).

This research used resources of the National Energy Research Scientific Computing Center (NERSC), a U.S. Department of Energy Office of Science User Facility located at Lawrence Berkeley National Laboratory, operated under Contract No. DE-AC02-05CH11231 using NERSC award HEP-ERCAP0023923.

This manuscript has been authored by Fermi Research Alliance, LLC under Contract No. DE-AC02-07CH11359 with the U.S. Department of Energy, Office of Science, Office of High Energy Physics.

Facilities: CTIO:4m, AAT

Software: `numpy` (Harris et al. 2020), `astropy` (Astropy Collaboration 2013, 2018), `matplotlib` (Hunter 2007), `pandas` (Pandas development team 2020), `scipy` (Virtanen et al. 2020), `SNANA` (Kessler et al. 2009), `Pippin` (Hinton & Brout 2020), `ChainConsumer` (Hinton 2016), `Source Extractor` (Bertin & Arnouts 1996), `MINUIT` (James & Roos 1975), SuperNNova (Möller & de Boissière 2020), SCONE (Qu et al. 2021).

APPENDIX

A. DATA RELEASE AND HOW TO USE THE DES-SN5YR DATA

All the input/output files necessary to reproduce our analysis and the outputs of our analysis pipeline are available on GitHub (https://github.com/des-science/DES-SN5YR).

The entire DES-SN5YR analysis used the SuperNova ANAlysis software (`SNANA`, Kessler et al. 2009),[13] integrated in the PIPPIN pipeline framework (Hinton & Brout 2020).[14] Both software packages are open-source and publicly available.

We release the PIPPIN input files necessary to *(i)* generate and fit all the simulations used in the analysis (both the large "biasCor" simulations to calculate bias corrections, and the DES-SN5YR-like simulated samples to validate the analysis); *(ii)* reproduce the full cosmological analysis, from light-curve fitting to photometric classification, distance estimates and cosmological fitting. Auxiliary files are also available within the SNANA library.[15]

The various (intermediate and final) *outputs* of our analysis pipeline are also provided at https://github.com/des-science/DES-SN5YR. This includes *(i)* light-curve fitted parameters, *(ii)* light-curve classification results, *(iii)* the final Hubble diagram and associated uncertainties covariance matrices, and *(iv)* the cosmology chains.

[13] https://github.com/RickKessler/SNANA

[14] https://github.com/dessn/Pippin

[15] Available on Zenodo https://zenodo.org/records/4015325.

REFERENCES

Alam, S., Ata, M., Bailey, S., et al. 2017, MNRAS, 470, 2617

Alam, S., Aubert, M., Avila, S., et al. 2021, PhRvD, 103, 083533

Alard, C. & Lupton, R. H. 1998, ApJ, 503, 325

Aleo, P. D., Malanchev, K., Sharief, S., et al. 2023, ApJS, 266, 9

Armstrong, P., Qu, H., Brout, D., et al. 2023, PASA, 40, e038

Astropy Collaboration. 2013, A&A, 558, A33

Astropy Collaboration. 2018, AJ, 156, 123

Bautista, J. E., Paviot, R., Vargas Magaña, M., et al. 2021, MNRAS, 500, 736

Bernstein, J. P., Kessler, R., Kuhlmann, S., et al. 2012, ApJ, 753, 152

Bertin, E. & Arnouts, S. 1996, A&AS, 117, 393

Betoule, M., Kessler, R., Guy, J., et al. 2014, A&A, 568, A22

Blanton, M. R., Bershady, M. A., Abolfathi, B., et al. 2017, AJ, 154, 28

Brout, D., Hinton, S. R., & Scolnic, D. 2021, ApJL, 912, L26

Brout, D. & Scolnic, D. 2021, ApJ, 909, 26

Brout, D., Scolnic, D., Kessler, R., et al. 2019a, ApJ, 874, 150

Brout, D., Sako, M., Scolnic, D., et al. 2019b, ApJ, 874, 106

Brout, D., Scolnic, D., Popovic, B., et al. 2022a, ApJ, 938, 110

Brout, D., Taylor, G., Scolnic, D., et al. 2022b, ApJ, 938, 111

Burke, D. L., Rykoff, E. S., Allam, S., et al. 2018, AJ, 155, 41

Camilleri, R., Davis, T., & the DES Collaboration. in prep. 2024

Chaboyer, B., Demarque, P., Kernan, P. J., & Krauss, L. M. 1998, ApJ, 494, 96

Chen, R. et al. 2022, ApJ, 938, 62

Chen, R., Scolnic, D., Rozo, E., et al. 2022, ApJ, 938, 62

Chevallier, M. & Polarski, D. 2001, IJMP D, 10, 213

Childress, M. J., Lidman, C., Davis, T. M., et al. 2017, MNRAS, 472, 273

Chotard, N., Gangler, E., Aldering, G., et al. 2011, A&A, 529, L4

Cimatti, A. & Moresco, M. 2023, ApJ, 953, 149

Conley, A., Guy, J., Sullivan, M., et al. 2011, ApJS, 192, 1

Dark Energy Survey Collaboration. 2016, MNRAS, 460, 1270

Dark Energy Survey Collaboration. 2019, ApJL, 872, L30

Dark Energy Survey Collaboration. 2022, PhRvD, 105, 023520

Dark Energy Survey Collaboration. 2023, PhRvD, 107, 083504

Dawson, K. S., Kneib, J.-P., Percival, W. J., et al. 2016, AJ, 151, 44

de Mattia, A., Ruhlmann-Kleider, V., Raichoor, A., et al. 2021, MNRAS, 501, 5616

Di Valentino, E., Mena, O., Pan, S., et al. 2021, Classical and Quantum Gravity, 38, 153001

Diehl, H. T., Neilsen, E., Gruendl, R., et al. 2016, in Society of Photo-Optical Instrumentation Engineers (SPIE) Conference Series, Vol. 9910, Observatory Operations: Strategies, Processes, and Systems VI, ed. A. B. Peck, R. L. Seaman, & C. R. Benn, 99101D

Dixon, M. et al. 2022, MNRAS, 517, 4291

du Mas des Bourboux, H., Rich, J., Font-Ribera, A., et al. 2020, ApJ, 901, 153

Duarte, J., González-Gaitán, S., Mourao, A., et al. 2022, arXiv e-prints, arXiv:2211.14291

Fioc, M. & Rocca-Volmerange, B. 1999, arXiv e-prints, astro

Foley, R. J., Scolnic, D., Rest, A., et al. 2017, MNRAS, 475, 193

Foreman-Mackey, D., Hogg, D. W., Lang, D., & Goodman, J. 2013, PASP, 125, 306

Ganeshalingam, M., Li, W., & Filippenko, A. V. 2013, MNRAS, 433, 2240

Gilliland, R. L., Nugent, P. E., & Phillips, M. M. 1999, ApJ, 521, 30

Gratton, R. G., Pecci, F. F., Carretta, E., et al. 1997, ApJ, 491, 749

Gupta, R. R., Kuhlmann, S., Kovacs, E., et al. 2016, AJ, 152, 154

Guy, J., Sullivan, M., Conley, A., et al. 2010, A&A, 523, A7

Handley, W. 2019, The Journal of Open Source Software, 4, 1414

Handley, W. & Lemos, P. 2019, PhRvD, 100, 023512

Handley, W. J., Hobson, M. P., & Lasenby, A. N. 2015, MNRAS, 450, L61

Harris, C. R., Millman, K. J., van der Walt, S. J., et al. 2020, Nature, 585, 357

Hicken, M., Challis, P., Jha, S., et al. 2009, ApJ, 700, 331

Hicken, M., Challis, P., Kirshner, R. P., et al. 2012, ApJS, 200, 12

Hinton, S. & Brout, D. 2020, Journal of Open Source Software, 5, 2122

Hinton, S. R. 2016, The Journal of Open Source Software, 1, 00045

Hlozek, R., Kunz, M., Bassett, B., et al. 2012, ApJ, 752, 79

Hou, J., Sánchez, A. G., Ross, A. J., et al. 2021, MNRAS, 500, 1201

Hunter, J. D. 2007, Computing in Science & Engineering, 9, 90

Ivezić, Ž., Kahn, S. M., Tyson, J. A., et al. 2019, ApJ, 873, 111

James, F. & Roos, M. 1975, Comput. Phys. Commun., 10, 343

Jeffreys, H. 1961, Theory of Probability, 3rd edn. (Oxford, England: Oxford)

Jennings, E., Wolf, R., & Sako, M. 2016, arXiv e-prints, arXiv:1611.03087

Jones, D. O., Scolnic, D. M., Riess, A. G., et al. 2018, ApJ, 857, 51

Jones, D. O., Scolnic, D. M., Foley, R. J., et al. 2019, ApJ, 881, 19

Jones, D. O., Foley, R. J., Narayan, G., et al. 2021, ApJ, 908, 143

Kelsey, L., Sullivan, M., Wiseman, P., et al. 2023, MNRAS, 519, 3046

Kenworthy, W. D., Jones, D. O., Dai, M., et al. 2021, ApJ, 923, 265

Kessler, R. & Scolnic, D. 2017, ApJ, 836, 56

Kessler, R., Vincenzi, M., & Armstrong, P. 2023, ApJL, 952, L8

Kessler, R., Bernstein, J. P., Cinabro, D., et al. 2009, PASP, 121, 1028–1035

Kessler, R., Marriner, J., Childress, M., et al. 2015, AJ, 150, 172

Kessler, R., Brout, D., D'Andrea, C. B., et al. 2019a, MNRAS, 485, 1171

Kessler, R., Narayan, G., Avelino, A., et al. 2019b, PASP, 131, 094501

Krisciunas, K., Contreras, C., Burns, C. R., et al. 2017, AJ, 154, 211

Kunz, M., Hlozek, R., Bassett, B. A., et al. 2012, Astrostatistical Challenges for the New Astronomy, 63–86

Lahav, O., Calder, L., Mayers, J., & Frieman, J. 2020, The Dark Energy Survey (Europe: World Scientific), https://www.worldscientific.com/doi/pdf/10.1142/q0247

Lasker, J., Kessler, R., Scolnic, D., et al. 2019, MNRAS, 485, 5329

Lee, J., Acevedo, M., Sako, M., et al. 2023, AJ, 165, 222

Lemos, P., Raveri, M., Campos, A., et al. 2021, MNRAS, 505, 6179

Lidman, C., Tucker, B. E., Davis, T. M., et al. 2020, MNRAS, 496, 19

Linder, E. V. 2003, PhRvL, 90, 091301

Marriner, J., Bernstein, J. P., Kessler, R., et al. 2011, ApJ, 740, 72

Meldorf, C., Palmese, A., Brout, D., et al. 2023, MNRAS, 518, 1985

Mitra, A., Kessler, R., More, S., Hlozek, R., & LSST Dark Energy Science Collaboration. 2023, ApJ, 944, 212

Möller, A. & de Boissière, T. 2020, MNRAS, 491, 4277

Möller, A., Smith, M., Sako, M., et al. 2022, MNRAS, 514, 5159

Möller, A. & the DES Collaboration. in prep. 2024

Pandas development team. 2020, Zenodo: pandas-dev/pandas: Pandas (https://doi.org/10.5281/zenodo.3509134)

Perlmutter, S., Aldering, G., Goldhaber, G., et al. 1999, ApJ, 517, 565

Planck Collaboration. 2020, A&A, 641, A6

Popovic, B., Brout, D., Kessler, R., & Scolnic, D. 2023a, ApJ, 945, 84

Popovic, B., Brout, D., Kessler, R., Scolnic, D., & Lu, L. 2021, ApJ, 913, 49

Popovic, B., Scolnic, D., Vincenzi, M., et al. 2023b, arXiv e-prints, arXiv:2309.05654

Prince, H. & Dunkley, J. 2019, PhRvD, 100, 083502

Qu, H., Sako, M., Möller, A., & Doux, C. 2021, AJ, 162, 67

Qu, H., Sako, M., Vincenzi, M., et al. 2023, arXiv e-prints, arXiv:2307.13696

Riess, A. G., Filippenko, A. V., Challis, P., et al. 1998, AJ, 116, 1009

Riess, A. G., Nugent, P. E., Gilliland, R. L., et al. 2001, ApJ, 560, 49

Riess, A. G., Strolger, L.-G., Tonry, J., et al. 2004, ApJ, 607, 665

Riess, A. G., Strolger, L.-G., Casertano, S., et al. 2007, ApJ, 659, 98

Riess, A. G., Rodney, S. A., Scolnic, D. M., et al. 2018, ApJ, 853, 126

Rose, B. M., Baltay, C., Hounsell, R., et al. 2021, arXiv e-prints, arXiv:2111.03081

Ross, A. J., Samushia, L., Howlett, C., et al. 2015, MNRAS, 449, 835

Rubin, D., Aldering, G., Betoule, M., et al. 2023, arXiv e-prints, arXiv:2311.12098

Ruhlmann-Kleider, V., Lidman, C., & Möller, A. 2022, JCAP, 2022, 065

Rykoff, E. S. 2023, Fermi Technical Note, FERMILAB-TM-2784-PPD-SCD

Sako, M., Bassett, B., Becker, A. C., et al. 2018, PASP, 130, 064002

Sánchez, B. O. in prep. 2024

Sánchez, B. O., Kessler, R., Scolnic, D., et al. 2022, ApJ, 934, 96

Scolnic, D., Brout, D., Carr, A., et al. 2022, ApJ, 938, 113

Scolnic, D. M., Jones, D. O., Rest, A., et al. 2018, ApJ, 859, 101

Sevilla-Noarbe, I., Bechtol, K., Kind, M. C., et al. 2021, ApJS, 254, 24

Smith, M., D'Andrea, C. B., Sullivan, M., et al. 2020a, AJ, 160, 267

Smith, M., Sullivan, M., Wiseman, P., et al. 2020b, MNRAS, 494, 4426

Smith et al. in prep. 2024

Stevens, A. R. H., Bellstedt, S., Elahi, P. J., & Murphy, M. T. 2020, Nature Astronomy, 4, 843

Sullivan, M., Le Borgne, D., Pritchet, C. J., et al. 2006, ApJ, 648, 868

Sullivan, M., Guy, J., Conley, A., et al. 2011, ApJ, 737, 102

Suzuki, N., Rubin, D., Lidman, C., et al. 2012, ApJ, 746, 85

Taylor, G., Jones, D. O., Popovic, B., et al. 2023, MNRAS, 520, 5209

The Dark Energy Survey Collaboration. 2005, arXiv e-prints, astro-ph/0510346, astro

Tripp, R. 1998, A&A, 331, 815

Trotta, R. 2008, Contemporary Physics, 49, 71

Valcin, D., Bernal, J. L., Jimenez, R., Verde, L., & Wandelt, B. D. 2020, JCAP, 2020, 002

VandenBerg, D. A., Bolte, M., & Stetson, P. B. 1996, Annual Review of Astronomy and Astrophysics, 34, 461

Vincenzi, M., Sullivan, M., Firth, R. E., et al. 2019, MNRAS, 489, 5802

Vincenzi, M. & The Dark Energy Survey. 2024, ApJ submitted

Vincenzi, M., Sullivan, M., Graur, O., et al. 2021, MNRAS, 505, 2819

Vincenzi, M., Sullivan, M., Möller, A., et al. 2023, MNRAS, 518, 1106

Virtanen, P., Gommers, R., Oliphant, T. E., et al. 2020, Nature Methods, 17, 261

Wiseman, P., Smith, M., Childress, M., et al. 2020, MNRAS, 495, 4040

Wiseman, P., Sullivan, M., Smith, M., et al. 2021, MNRAS, 506, 3330

Wiseman, P., Vincenzi, M., Sullivan, M., et al. 2022, MNRAS, 515, 4587

Ying, J. M., Chaboyer, B., Boudreaux, E. M., et al. 2023, AJ, 166, 18

Yuan, F., Lidman, C., Davis, T. M., et al. 2015, MNRAS, 452, 3047

Zuntz, J., Paterno, M., Jennings, E., et al. 2015, Astronomy and Computing, 12, 45